THE ASTROPHYSICAL JOURNAL, 345:939–958, 1989 October 15


# THEORETICAL MODELS OF VERY LOW MASS STARS AND BROWN DWARFS

ADAM BURROWS
Departments of Physics and Astronomy, University of Arizona
AND
W. B. HUBBARD AND JONATHAN I. LUNINE
Lunar and Planetary Laboratory, University of Arizona
*Received 1988 December 10; accepted 1989 April 19*

## ABSTRACT

We present the results of a new series of stellar evolution calculations for very low mass stars ($\lesssim 0.2\ M_\odot$) and brown dwarfs ($< 0.08\ M_\odot$). We investigate the dependence of the effective temperatures, luminosities, radii, etc., on the mixing length, the atmospheric opacities, and the helium fraction, along the very low mass star/brown dwarf continuum. Numerical data tables, isochrones, and evolutionary curves of the various observables and structural quantities are presented for seven models of fifteen masses each, between 0.03 $M_\odot$ and 0.2 $M_\odot$. In this way, the physics of the transition region between stars and brown dwarfs is explored in a self-consistent way. We compare our results with recent data from Liebert and Probst, McCarthy *et al.*, Becklin and Zuckerman, and Berriman and Reid and find reasonable agreement. The status of both theory and observation for this problematic class of low luminosity, infrared objects is discussed.

*Subject headings:* stars: evolution — stars: interiors

## I. INTRODUCTION

Very low mass (VLM) stars ($0.08\ M_\odot < M < 0.3\ M_\odot$) dominate the solar neighborhood ($< 10$ pc) and constitute the most numerous stellar component of the Galaxy. Indeed, they, along with substellar ($\lesssim 0.08\ M_\odot$) "brown dwarfs" that do not reach the hydrogen main sequence, may be responsible for the dynamically inferred missing mass of the local and/or the Galactic disk (Oort 1960; Bahcall 1986) and might account for the mass sinks in X-ray cooling flows (Sarazin and O'Connell 1983). However, in order to account for this missing mass, there must be a sharp increase in the mass function below $\sim 0.1\ M_\odot$ that has yet to be demonstrated (Hawkins 1986; Scalo 1986; Reid 1987; Liebert and Probst 1987, hereafter LP87). The foremost obstacle to the study of VLMs and brown dwarfs is their low luminosity ($L = 10^{-2}$ to $10^{-6}\ L_\odot$), which, due to their low surface temperatures ($T_e \lesssim 3000$ K), is predominantly in the infrared bands ($J$[1.2 $\mu$m], $H$[1.6 $\mu$m], $K$[2.2 $\mu$m], $L$[3.5 $\mu$m], and $M$[5.0 $\mu$m]), for which there have only recently been developed adequate detectors.

The classic surveys by Luyten (1963, 1976*a*, *b*), Giclas (1958), and Gliese (1969) have been the foundation of M dwarf astronomy. However, the new technology (sensitive emulsions, CCDs, cryostats, measuring machines, computers, etc.) is forcing a renaissance in the study of dim red-infrared objects. The photometry of Reid and Gilmore (1984) and Becklin and Zuckerman (1988, hereafter BZ88), the spectrophotometry of Berriman and Reid (1987, hereafter BR87), the speckle work of McCarthy *et al.* (1988*a*, *b* [hereafter Mc88] and references therein), and the compilations of LP87, among others, are beginning to yield luminosity functions, luminosities, radii, temperatures, and spectra in the VLM/brown dwarf (BD) mass range (see Table 1 and Fig. 1). Furthermore, Zuckerman and Becklin (1988) claim to have identified a brown dwarf companion as an IR excess to the white dwarf Giclas 29–38, and Becklin and Zuckerman (1988) have recently announced similar excesses in GD 165 and seven more of the 100 white dwarfs they have surveyed. Forrest, Skrutskie, and Shure (1988) have found an IR companion to Gliese 569 (Giclas 136–28) that, if not a brown dwarf, is a very late M dwarf near the main-sequence edge. Wade and Horne (1988) have determined the mass ($\sim 0.083\ M_\odot$) and radius ($\sim 0.15\ R_\odot$) of the low-mass secondary in the dwarf nova system Z Cha, and Fruchter *et al.* (1988) have deduced similar quantities ($M = 0.022\ M_\odot$, $R = 0.15\ R_\odot$) for the companion of the millisecond, eclipsing, binary pulsar, PSR 1957+20. This flurry of observations of low mass objects and the anticipated launch of the Hubble Space Telescope (HST) and the Space Infrared Telescope Facility (SIRTF) (in the mid-1990s), each of which should yield deep, complete samples of VLMs, suggest that the time is ripe for a new set of detailed calculations of the evolution and properties of objects in the VLM/BD mass range.

The theory of VLMs and low-mass stars ($\lesssim 0.7\ M_\odot$) has a long pedigree (Kumar 1963*a*, *b*; Grossman, Hays, and Graboske 1974, hereafter G74; Vandenberg *et al.* 1983, hereafter V83; D'Antona and Mazzitelli 1985, hereafter DM85; Stringfellow 1986) and has been successful in detail only beyond the upper margin of the VLM range, i.e., above 0.3 $M_\odot$. Below 0.3 $M_\odot$, the inferred radii and effective temperatures ($T_e$) in particular, have been problematic, and an acceptable fit to the observational H-R diagram has been elusive. An adequate theory must incorporate (1) a good equation of state (EOS) from the molecular hydrogen phase, through the molecular dissociation and ionization regions, to the metallic H/He region; (2) a detailed treatment of the atmospheric opacities for $T_e$ below 3500 K and gravities in the $10^5$ cm s$^{-2}$ range; and (3) nuclear rates suited to the "low" ($< 7 \times 10^6$ K) central temperature ($T_c$), high central density ($2000\ \text{g cm}^{-3} > \rho_c > 100\ \text{g cm}^{-3}$) regimes encountered along the VLM/BD continuum. All of the contributing theorists to date have been aware of the importance of the above three ingredients and are in substantive agreement on the predicted properties of the objects for which their respective studies overlap. It may well be that there are

TABLE 1

VLM DATA

| Object | $M_{bol}$ | log $T_e$ (K) | $M/M_\odot$ | Comments |
|---|---|---|---|---|
| | | Liebert and Probst 1987 [$M_{bol}(\odot) = 4.70$][a] | | |
| GL 53B ..... | 10.1 ± 0.2 | 3.497 ± 0.015 | 0.19 ± 0.02 | $\mu$ Cas B |
| GL 65A ..... | 11.7 ± 0.1 | 3.440 ± 0.013 | 0.115 ± 0.008 | L726-8A |
| GL 65B ..... | 12.2 ± 0.1 | 3.426 ± 0.013 | 0.109 ± 0.008 | L726-8B |
| GL 166C ..... | 10.3 ± 0.1 | 3.486 ± 0.013 | 0.16 ± 0.01 | $o^2$ Eri C |
| GL 234B ..... | 12.2 ± 0.1 | 3.42 ± 0.02 | 0.08 ± 0.01 | Ross 614B |
| GL 473AB ..... | 11.5 ± 0.1 | 3.442 ± 0.013 | 0.065 ± 0.02 | Wolf 424AB, double, assumed same mass |
| GL 623B ..... | 12.3 ± 0.2 | 3.42 ± 0.02 | 0.09 ± 0.03 | McCarthy *et al.* 1988; Marcy and Moore 1989 |
| GL 748B ..... | 10.8 ± 0.2 | 3.47 ± 0.02 | 0.10 ± 0.04 | Wolf 1062 |
| GL 860B ..... | 10.8 ± 0.1 | 3.447 ± 0.013 | 0.16 ± 0.01 | Kruger 60B |
| GL 896B ..... | 10.2 ± 0.1 | 3.46 ± 0.02 | 0.16 ± 0.03 | |
| GL 866A ..... | 11.2 | 3.42 | 0.13 | McCarthy, Cobb, and Probst 1987; |
| GL 866B ..... | 11.8 | 3.42 | 0.11 | Berriman and Reid 1987 |
| | | B. McCarthy *et al.* 1988*b* | | |
| G 208-44A ..... | 11.8 ± 0.1 | ... | 0.14 ± 0.03 | |
| G 208-44B ..... | 13.1 ± 0.1 | ... | 0.10 ± 0.02 | |
| | | C. Berriman and Reid 1987 [$M_{bol}(\odot) = 4.64$] | | |
| GJ 1111 ..... | 12.37 | 3.389 | ... | |
| GL 406 ..... | 12.1 | 3.415 | ... | Wolf 359 |
| GL 411 ..... | 8.82 | 3.512 | ... | |
| GL 447 ..... | 10.57 | 3.505 | ... | |
| GL 643 ..... | 10.44 | 3.498 | ... | |
| GL 644C ..... | 12.84 | 3.389 | ... | VB 8; see also Reid and Gilmore 1984 |
| GL 699 ..... | 10.89 | 3.491 | ... | Barnard's star |
| GL 752A ..... | 8.39 | 3.508 | ... | |
| GL 821 ..... | 9.19 | 3.544 | ... | |
| GL 884 ..... | 7.34 | 3.562 | ... | |
| LHS 2924 ..... | 14.19 | 3.29 | ... | see Probst and Liebert 1983 ($M_V = 19$) |
| | | D. Becklin and Zuckerman 1988 | | |
| GD 165B ..... | 14.97 | 3.328 | ... | |
| LHS 2924 ..... | 13.37 | 3.447 | ... | see BR87 above |
| GL 569B ..... | 12.53 | 3.443 | ... | |
| VB 8 ..... | 12.59 | 3.491 | ... | see BR87 above |
| VB 10 ..... | 12.79 | 3.477 | ... | |

[a] As modified by McCarthy *et al.* 1988*b*.

systematic errors in the observed masses, $T_e$'s, and ages that will explain the discrepancies between hard-won data and long-standing theory (see § III*b*).

In this paper, we investigate afresh the theory of "stars" in the 0.03–0.2 $M_\odot$ range. We place special emphasis on comparisons between our calculations and the recent data (Table 1 and Fig. 1), and on the effect of varying the opacity, helium fraction ($Y_\alpha$), and mixing length ($l$) parameter ($\alpha = l/H_p$, where $H_p$ = the pressure scale height). Furthermore, with graphs and tables, we present model results that can be compared conveniently with the growing store of data on VLMs and brown dwarfs. Following many others (see references above), we derive the minimum hydrogen main-sequence mass, effective temperature, and luminosity, determine on what these quantities depend, and follow the evolution of both VLMs and brown dwarfs for 20 Gyr. This study is a continuation of our work on brown dwarfs (Lunine *et al.* 1989, hereafter Paper I) and was undertaken in part to address the transition region from brown dwarfs to VLMs in a consistent and detailed fashion and to determine what is required to reconcile theory with observation.

## II. METHODS AND INPUT PHYSICS

The Lagrangian Henyey routine employed for these simulations is described in Paper I and Burrows and Lattimer (1986). The code uses a predictor-corrector algorithm to achieve second-order accuracy in time, employs detailed atmosphere and EOS grids to speed calculation and is fully implicit. On the Vax 8650 on which the models were run, between 8 minutes and 1 hr of CPU time was required for each 20 Gyr run. The time step was chosen to ensure that in none of the 120 radial zones did the temperature change by more than 1% per cycle. The atmospheric (radiative) skin is so thin ($\Delta R/R < 10^{-4}$, $\Delta M \sim 10^{-10}\ M_\odot$) that a dynamic range in the mass zoning of eight orders of magnitude was required. Otherwise, the "stars" of this study ($0.03\ M_\odot < M < 0.2\ M_\odot$) are fully convective. Those massive enough to land on the hydrogen main sequence would stay there for at least 100 Gyr, most for far longer. For these stars, since the age of the Galaxy is no more than 20 Gyr, evolution beyond, and even on, the main sequence is slow and only of academic interest. For the brown dwarfs that do not

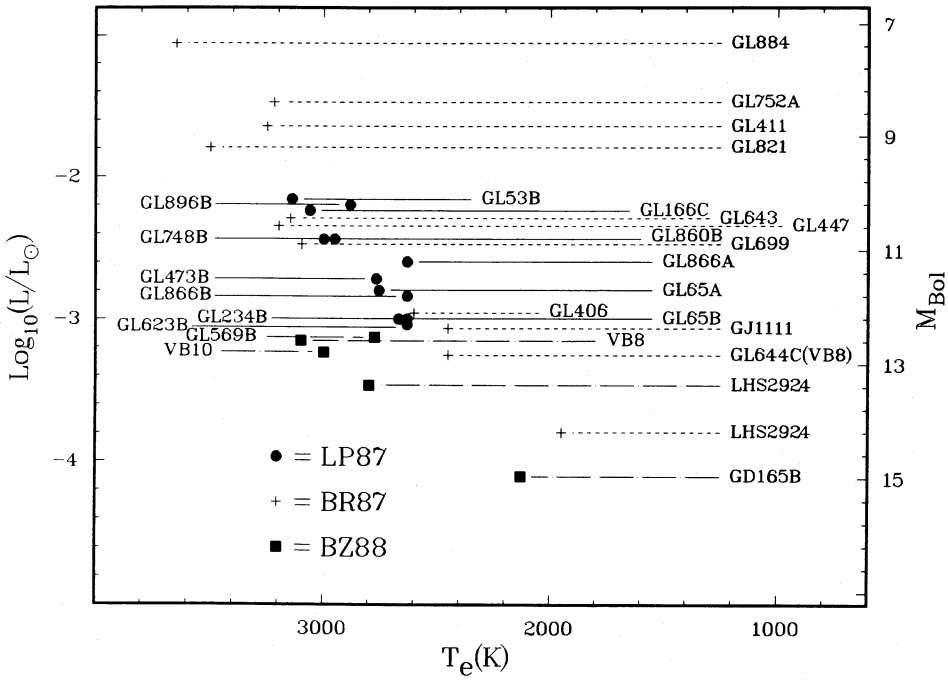


FIG. 1.—Luminosity ($L$, in units of $L_\odot$) and $M_{bol}$ [$M_{bol}(\odot) = 4.70$] vs. effective temperature, $T_e$, for the Liebert and Probst (1987, LP87) data, as modified by McCarthy *et al.* (1988*b*), for the Berriman and Reid (1987, BR87) data, and for the Becklin and Zuckerman (1988, BZ88) data. The Gliese numbers are connected to the points by lines (*dashed lines*, BR87; *solid lines*, LP87; *dashed-dot*, BZ88). This H-R diagram contains the objects from Table 1 for which both $L$ and $T_e$ are available. Dim, low-temperature objects are in the lower right and the brighter, hotter objects are in the upper left.

ignite a significant amount of hydrogen during their Kelvin-Helmholtz contraction ($M \lesssim 0.06\ M_\odot$), 20 Gyr is ample time for them to cool into obscurity ($T_e < 600$ K). It was these considerations that led us to simulate only the first 20 Gyr of VLM/BD evolution.

### *a) Nuclear Processes*

The thermonuclear processes relevant at the temperatures and densities in the VLM/BD regime are

$$p + p \rightarrow d + e^+ + \nu_e\ , \quad \text{where} \quad Q_p = 1.442\ \text{MeV} \qquad (1)$$

and

$$p + d \rightarrow {}^3\text{He} + \gamma\ , \quad \text{where} \quad Q_d = 5.494\ \text{MeV}\ . \qquad (2)$$

Reaction (1) is the rate-limiting process, as it proceeds by the weak interaction. The rates for these proton- and deuterium-burning reactions were obtained from Fowler, Caughlan, and Zimmerman (1975, hereafter FCZ). At the high densities ($\rho_c \sim$ 100–2000 g cm$^{-3}$) and "low" temperatures ($T_c \sim$ [2–6] $\times 10^6$ K) reached by VLMs, the Coulomb parameter, $\Gamma$ ($= Z^2e^2/r_i kT$), is of order unity. Hence, the screening corrections to the thermonuclear rates on the hydrogen main sequence are not negligible ($\sim$1.1–2.0), and we have used the intermediate screening algorithm of Graboske *et al.* (1973) to calculate them. The temperature dependence of the corrected FCZ rate of reaction (1) in the VLM central temperature regime is strong and roughly $\propto T^{6\text{-}8}$. Pycnonuclear rates for all the densities encountered in this study are negligible and were ignored.

Since $T_c$ does not exceed $\sim 6 \times 10^6$ K for $M < 0.2\ M_\odot$, $^3$He does not accumulate rapidly. The low $^3$He fraction and temperatures inhibit $^3$He-burning by the processes $^3$He($^3$He, $2p$)$^4$He and $^3$He($^4$He, $\gamma$)$^7$Be of the standard $p$-$p$ chain. As a consequence, $^3$He takes much longer than 20 Gyr to reach equilibrium and the p-p chain is truncated. The effective $Q$ is not the 13.8 MeV per reaction (1) of the p-p I chain, but 12.16 MeV per reaction (1) and only reactions (1) and (2) are important. Primordial deuterium will burn at low temperatures ($\sim 5 \times 10^5$ K) by reaction (2), but this "deuterium main-sequence" phase lasts no more than $\sim 10^7$ yr for VLM/BDs, does not significantly alter or enliven VLM/BD evolution (Grossman 1970; Lunine, Hubbard, and Marley 1986), and will not be highlighted in this paper.

### *b) Equation of State*

As is well known, brown dwarfs are characterized by thermodynamic conditions in which the deep interior is a strongly coupled liquid of pressure-ionized hydrogen and helium nuclei, together with degenerate electrons. The outermost layers of brown dwarfs, which are discussed in § II*c*, are weakly coupled and can be treated with the standard statistical mechanical description of ideal gases with internal degrees of freedom.

Figure 2 provides an orientation to the relevant regions of the hydrogen phase diagram. The lower part of this figure shows various phase boundaries in pure hydrogen, as presented by Marley and Hubbard (1988). At pressures, $P$, lower than about 3 Mbar, molecular hydrogen is stable and exists in either the liquid or solid phase. To the right of the near-vertical phase boundary at 3–5 Mbar, there are two phases of metallic hydrogen: liquid and solid. The phase boundary between liquid molecular hydrogen and liquid metallic hydrogen (marked MH) is shown in two versions, and corresponds to two different assumptions about the effect of pressure on the internal degrees of freedom of an $H_2$ molecule (Marley and Hubbard 1988). The phase boundaries terminate at high temperatures

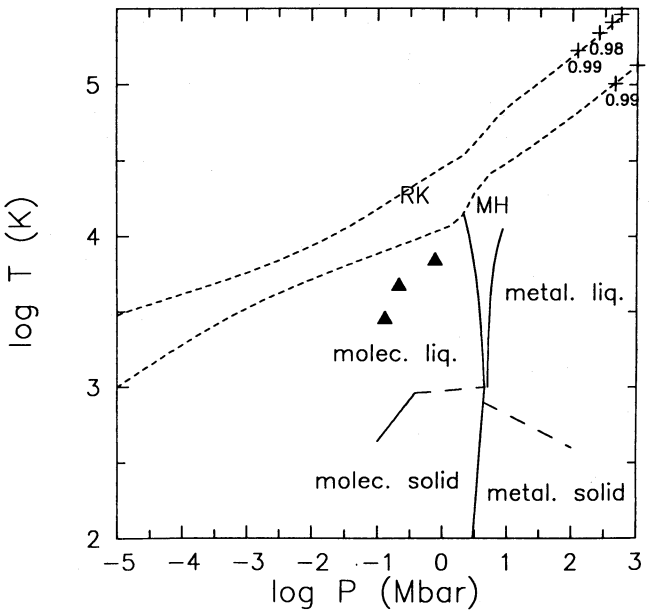


FIG. 2.—Phase diagram for hydrogen at high pressures and temperatures, together with two interior trajectories for typical brown dwarf models. See text for discussion.

where the model of Marley and Hubbard is unreliable, and not necessarily at a critical point. On the other hand, the theory of Robnik and Kundt (1983) does predict a critical point at the position marked RK. According to this alternate theory, the phase boundaries calculated by Marley and Hubbard would extend to and terminate at the point RK instead of the point MH. However, it is important to note that the phase boundary calculated by Marley and Hubbard is determined self-consistently from a free-energy fit to the experimental shock compression points of Nellis *et al.* (1983) on $H_2$ (*triangles*), and thus is calibrated to experimental data. The equations of state used in this paper are consistent with these data.

The two dashed trajectories in the upper part of Figure 2 show two typical brown dwarf models. The upper curve is for a brown dwarf of 0.05 $M_\odot$ and $T_{10} = 3000$ K, while the lower curve is for a brown dwarf of the same mass but with $T_{10} =$ 1000 K. ($T_{10}$ is the temperature at the 10 bar pressure level.) The labeled points on these curves show the fractional mass enclosed within a point at the indicated pressure. Thus, more than 99% of the brown dwarf mass is in the liquid metallic hydrogen phase. The outermost 1% of the mass has, for the most part, poorly understood thermodynamic properties. However, the entropy of the brown dwarf is established by the radiative and convective properties of the atmosphere, where the gas thermodynamics departs only slightly from ideality.

The thermodynamics of a mixture of hydrogen and helium is calculated as follows. In the molecular-liquid region, we use the expressions of Marley and Hubbard, with

$$F = F_0 + F_{\rm int} , \tag{3}$$

where $F_0$ is the ideal gas free energy of a mixture of hydrogen and helium, and $F_{\rm int}$ is an interaction free energy calibrated to the shock data. We include thermal molecular dissociation and ionization in $F_0$.

In the metallic hydrogen region, we use a generalization of the expression of Hubbard and De Witt (1985):

$$F = F_0 + F_e + F_{\rm int} , \tag{4}$$

where $F_0$ is now the Helmholtz free energy of an ideal gas of hydrogen and helium nuclei, $F_e$ is the Helmholtz free energy of an ideal gas of free, partially degenerate electrons plus the first-order finite-temperature exchange Helmholtz free energy of free electrons, and $F_{\rm int}$ is the interaction free energy obtained by Hubbard and DeWitt.

No attempt is made to bridge the gap between expressions (3) and (4). Instead, we carry out an interpolation of thermodynamic quantities between the two phases and ensure that the entropy is calculated on a consistent zero point in the two regions. As indicated in Figure 2, virtually all of the mass of the brown dwarf will be in the liquid metallic hydrogen phase, and it is in this region that a careful physical treatment is most essential. The only case in which the thermodynamics of intermediate regions would become important is if the brown dwarf interior crosses a phase boundary, which could lead to an entropy mismatch between the deep interior and the atmospheric regions. As shown in Figure 2, this situation could occur if the Robnik and Kundt theory is correct. However, the available experimental data do not provide any confirmation for this hypothesis, and we proceed under the assumption that the metallization of hydrogen at temperatures prevailing in brown dwarfs occurs continuously.

Our theory differs in important respects from some earlier theories which have been used in studies of brown dwarfs. Examples of these are Magni and Mazzitelli (1979, hereafter MM), and Fontaine, Graboske, and Van Horn (1977, hereafter FGVH). In both of these theories, considerable attention is given to deriving a thermodynamically consistent treatment of the region of partial thermal and pressure ionization and dissociation, although neither theory is tied to experimental data. The treatment of the liquid metallic hydrogen region in both the MM and FGVH theories is somewhat cruder than our theory. In this region, both MM and FGVH use a finite-temperature Thomas-Fermi approach, which assumes that the protons and alpha particles are in a perfect crystal rather than in a liquid state. Thus MM and FGVH have probably somewhat overestimated the Coulomb corrections to the thermodynamics in this regime, but the error may not be a serious one. Since the Coulomb correction is the largest nonideal contribution to the equations of state in the liquid metallic hydrogen regime, differences in treatment of other terms should not lead to serious discrepancies.

We have not carried out a quantitative comparison of our thermodynamics with that of MM or FGVH, but would expect on the basis of the above remarks that our pressure-density relations should be very similar to theirs, and thus our brown dwarf radii should be correspondingly similar for the same values of the mass and interior entropy. On the other hand, quantities which are more sensitive to the treatment of the proton liquid, such as thermal corrections to the radii and heat capacities, could well differ by some tens of percent. This could have a significant effect on cooling ages of brown dwarfs, but will little affect the lower density, higher entropy VLMs.

Rather than call our long equation-of-state subroutine every cycle of the evolutionary calculations, we construct two tables (each 100 × 330), one of entropy and the other of pressure for 100 temperatures and 330 densities that span the thermodynamic space encountered by brown dwarfs and VLM's. During a simulation, the program quickly obtains all relevant thermodynamic quantities from these tables by six-point interpolation and numerical differentiation (e.g., to obtain specific heats). In practice, this approach speeds up our runs by more than a factor of 10.

### c) *Atmosphere Models and Opacities*

The temperature-pressure structure of the outer envelope, referred to here as the atmosphere, provides a value for the entropy of the interior for a specified effective temperature, surface gravity, and composition. The entropy is determined by the temperature and pressure point at which the atmosphere is adiabatic, that is, where essentially all of the internal heat flux is carried outward by convection as opposed to radiation. For a given composition, we compute a grid of atmosphere models in effective temperature-surface gravity space to construct an interpolation table of interior entropies. The utility of this approach is evident: a grid of atmosphere models need only be calculated once to handle all sequences of evolutionary models of brown and red dwarfs. In practice, uncertainties in the treatment of gas opacity, grain formation and opacity, and the efficiency of convective transport force the construction of a number of atmosphere tables. In this section, we describe the treatment of these physical parameters and processes.

Because of the large number of models which need to be calculated for a grid of atmospheres (generally four surface gravities from $10^4$ to $3 \times 10^5$ cm s$^{-2}$ and 20 effective temperatures from 600 to 4000 K), and the large number of pressure levels ($10^3$–$10^4$) required to treat grain formation and convective inefficiency, a gray atmosphere formalism is used. The equations are the same as those used in Paper I and will not be repeated here. A major departure from the first paper is the need to explicitly calculate the flux carried outward by convection and radiation in the atmospheric regime in which the radiative temperature gradient is superadiabatic. Models with effective temperatures above 2400 K are rather sensitive to the efficiency of convection, since the region of the atmosphere in which convection takes over from radiation is that in which hydrogen dissociation and ionization take place.

In the absence of specific knowledge of the presence or effect of surface magnetic fields or rotation, we employ a mixing-length formalism to compute the temperature gradient in convective regions of the atmosphere. The formalism assumes that there is a typical length scale (the mixing length) over which buoyant parcels of gas (convective "bubbles") can transport heat upward before they dissolve into their surroundings. The assumption of Paper I, that the temperature gradient never exceeds the adiabat anywhere within the model, corresponds to the case of infinite mixing length. In the limit of zero mixing length, the atmospheric temperature gradient must be purely radiative. A typical mixing length chosen in models of the solar photosphere is 1.5 pressure scale heights (i.e., $\alpha = 1.5$; see, for example, Vandenberg and Bridges 1984).

The planet Jupiter, with a mass near $10^{-3}\ M_\odot$, can be thought of as an extremely light brown dwarf. Deeper than five bars in the Jovian atmosphere, the internal energy flux is evidently transported outward by convection; however, a good measurement of the temperature gradient in that region awaits the Galileo entry probe. There is some evidence that in Jupiter moist convective processes extend over roughly a scale height (Lunine and Hunten 1987). The upwelling, high-velocity plumes correspond to a mixing-length parameter well in excess of unity, gently sinking regions to a mixing length much smaller than unity. This illustrates the limitations of assigning a single mixing length to Jovian tropospheric convection. Nonetheless, recent calculations by Del Genio and McGratten (1988), based on parameterized cumulus convection models developed for Earth, predict that moist convection on Jupiter breaks up into thin layers whose vertical extent is ~10% of the scale height. This suggests that an appropriate mixing length parameter for Jupiter's troposphere is ~0.1. While this calculation applies to moist convection in which positive buoyancy due to latent heat is partially negated by the high molecular weight of water relative to hydrogen, it may well be relevant to our stellar models in the 2400–3000 K effective temperature range, in which hydrogen recombination ($H + H \rightarrow H_2$) in upwelling parcels produces latent heat and negatively buoyant hydrogen molecules.

The mixing length model of convection is taken directly from Mihalas (1978); the relevant equations will not be reproduced here. The calculation depends sensitively on the values of the radiative and adiabatic temperature gradients. The radiative gradient is calculated using the opacities described below; the adiabatic gradient determination uses the hydrogen-helium equation of state explained in § 11*b*. A look-up table was created from the calculation of the adiabat to permit the adiabatic temperature gradient to be determined for each of the pressure levels in each atmosphere model. The departure from adiabatic convection is most pronounced at low optical depths in the atmosphere. The approach to adiabatic convection is rapid at effective temperatures below 2400 K but increasingly sluggish above that. The resulting effect of the mixing-length model on the temperature profile is shown in Figure 3 for two effective temperatures and three mixing lengths. As noted above, the low effective temperature models are insensitive to changes in the mixing length; at higher effective temperature, the adiabatic temperature gradient is significantly lower than the radiative gradient at modest optical depths, leading to substantial departures from adiabaticity and a marked sensitivity

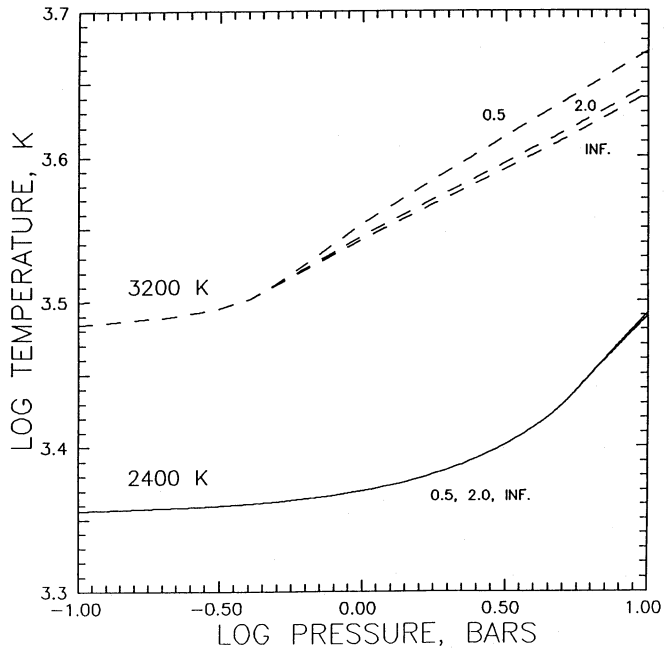


FIG. 3.—Effect of mixing length on the temperature-pressure profile for the high gas opacity model described in the text. Effective temperature is given next to each set of profiles; mixing length in units of pressure scale height is also indicated. For the lower curves, all three profiles essentially overlap. The surface gravity is $10^5$ cm s$^{-2}$.

to mixing length. In fact, the smallest mixing length produces convection so inefficient that fully adiabatic convection is still not achieved at temperatures well above $10^4$ K, for which the opacities used are no longer valid. Hence, the models involving the smallest mixing length somewhat underestimate the effect of the mixing length on the interior entropy, since they are arbitrarily brought onto an adiabat when the temperature has gone well beyond the range of validity of the opacity tables.

The atmosphere models reported on here span an enormous range of temperature and pressure, from 500 to over 10,000 K in temperature, and 0.1 to 100 bar in pressure. In this range, the dominant source of opacity shifts from pressure-induced hydrogen-helium absorption and molecular line transitions to $H^-$ absorption. The mechanism determining the line width in water and carbon monoxide absorption likewise changes from pressure broadening to thermal (Doppler) broadening. To treat these processes in detail would be prohibitive in light of the large number of atmosphere models required. Hence, we use the scheme adopted in Paper I, namely frequency-averaged absorption coefficients calculated by Tsuji (1971) for a range of pressures from $10^{-5}$ bar to 1000 bar, and temperatures from 500 to 4000 K. A full description of Tsuji's opacities is provided in Paper I. As previously, we take two cases: a "high" gas opacity which includes all molecular sources, and a "low" gas opacity which includes only the hydrogen-helium opacity. Resulting temperature profiles for these two cases are shown in Figure 4 for an effective temperature of 2400 K.

Because our new models extend to much higher temperatures than the previous study, it was also necessary to consider a set of opacities more appropriate to the high temperature, doppler-broadened limit. Hence, we also used Rosseland mean opacities for a solar composition atmosphere computed by Alexander, Johnson, and Rypma (1983), valid for densities from $10^{-18}$ to $10^{-12}$ g cm$^{-3}$ at 600 K and $10^{-11}$ to $10^{-2}$ g cm$^{-3}$ at 10,000 K. A temperature profile using this opacity scheme is also shown in Figure 4; it yields stellar models very similar to the high (*H*) opacity case. Alexander, Johnson, and Rypma (1983) provide auxiliary tables for a range of helium abundances; in the temperature-pressure regime of our models, the variation of opacity due to $Y_\alpha$ changes from 0.22 to 0.25 is generally less than 10%. Finally, Alexander (1989) has revised his Rosseland mean opacities downward; consequently, we assert that our opacity choices (*H*, *L*, and Alexander, Johnson, and Rypma 1983) provide a sufficient range to bracket the gas opacity. We prefer the Alexander, Johnson, and Rypma (1983) opacities to the 1989 tabulation because the former are used by D'Antona and Mazzitelli (1985), allowing the direct comparison of stellar models in § III.

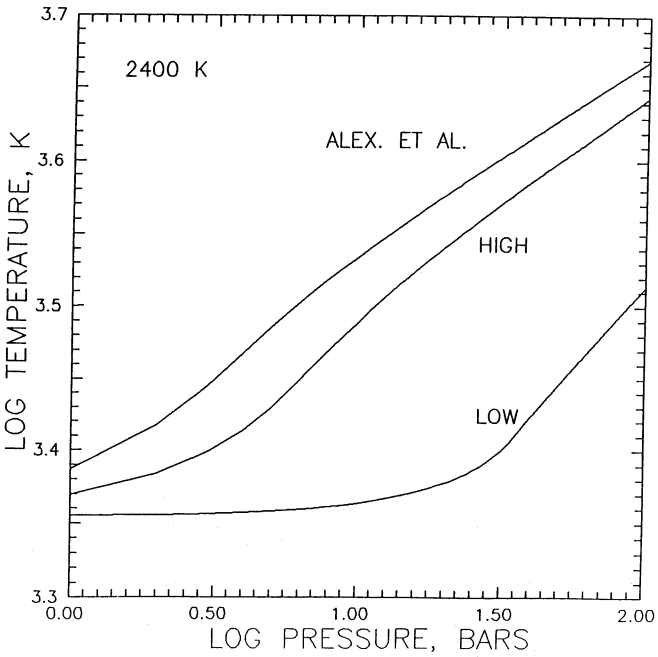


FIG. 4.—Temperature-pressure profiles in the atmosphere for three choices of gas opacity: low (*L*), high (*H*), and Alexander, Johnson, and Rypma (1983). The last two cases also include the so-called condensation cloud model described in the text. Surface gravity is $10^5$ cm s$^{-2}$; the mixing-length parameter, $\alpha$, is set equal to $\infty$.

Silicate and iron grains can significantly contribute to the total opacity over a range of effective temperatures from 1400 K up to 2400 K. The construction of models of grain size and vertical distribution was a focus of Paper I. We use the cloud models described therein. In particular, to limit the number of stellar models presented below, we focus on the so-called condensation cloud case of Paper I, with a small modal grain size (0.1 $\mu$m). This tends to maximize the effect of clouds on the temperature profile. As described in Paper I, other particle sizes and vertical distributions yield temperature-pressure profiles either similar to this case or intermediate between this and the no-cloud (pure gas opacity) model.

In the preceding paragraphs, we have outlined a range of atmosphere models with varying convective efficiency, gas opacity, and absorption due to grains. Each model atmosphere was calculated using 1000 pressure levels. Experimental runs with 10,000 pressure levels yielded identical results to those with 1000 levels. In Table 2, we list the atmosphere models used to construct our stellar models along with their labels used in later figures. In picking this range, we have attempted to bracket the various physical effects the atmospheric temperature-pressure profile may have on the interior entropy, while restricting ourselves to conditions which we regard as physically reasonable in the stellar objects considered in this paper. The resulting atmospheric temperature-pressure profiles compare well to those presented in Cox, Shaviv, and Hodson (1981), with the proviso that some of the properties of their model are incompletely described. The results presented below indicate that the models are much less sensitive to the opacity than they are to the convective efficiency (mixing length). We therefore regard our treatment of the opacity as satisfactory for the present problem, though more detailed treatments are justified when generating spectra (work in progress).

TABLE 2

LIST OF MODELS

| Model | Gas Opacity | $\alpha = l/H_p$ | $Y_\alpha$ |
|---|---|---|---|
| A..... | High, clouds | $\infty$ | 0.22 |
| B..... | High, clouds | 1.0 | 0.22 |
| C..... | High, clouds | 0.5 | 0.22 |
| D..... | High, clouds | 0.1 | 0.22 |
| E..... | Low, no clouds | 0.5 | 0.22 |
| F..... | Alexander *et al.* 1983, clouds | $\infty$ | 0.22 |
| G..... | High, clouds | 1.0 | 0.25 |

1989ApJ...345..939B

TABLE 3

MODEL A[a]

| Mass ($M_\odot$) | Age ($10^9$ yrs) | $T_e$(K) | Lum ($L_\odot$) | Rad ($10^9$ cm) | $T_c$ ($10^6$) | $\rho_c$ | S | $L_n/L$ |
|---|---|---|---|---|---|---|---|---|
| 0.200 | 10.0 | 3620.0 | 0.729E-02 | 15.10 | 6.080 | 153.0 | 13.21 | 1.000 |
| 0.150 | 10.0 | 3430.0 | 0.378E-02 | 12.10 | 5.350 | 218.0 | 12.33 | 1.000 |
| 0.125 | 0.1 | 3320.0 | 0.302E-02 | 11.50 | 4.560 | 210.0 | 12.02 | 0.381 |
| | 1.0 | 3270.0 | 0.232E-02 | 10.50 | 4.840 | 282.0 | 11.71 | 0.996 |
| | 10.0 | 3270.0 | 0.232E-02 | 10.40 | 4.840 | 283.0 | 11.71 | 1.000 |
| 0.110 | 0.1 | 3240.0 | 0.248E-02 | 11.00 | 4.090 | 212.0 | 11.75 | 0.210 |
| | 1.0 | 3170.0 | 0.161E-02 | 9.27 | 4.460 | 353.0 | 11.19 | 0.988 |
| | 10.0 | 3170.0 | 0.160E-02 | 9.25 | 4.460 | 355.0 | 11.18 | 1.000 |
| 0.100 | 0.1 | 3190.0 | 0.217E-02 | 10.60 | 3.750 | 212.0 | 11.56 | 0.125 |
| | 1.0 | 3050.0 | 0.113E-02 | 8.39 | 4.120 | 430.0 | 10.73 | 0.974 |
| | 10.0 | 3040.0 | 0.111E-02 | 8.36 | 4.120 | 435.0 | 10.72 | 1.000 |
| 0.095 | 0.1 | 3160.0 | 0.202E-02 | 10.40 | 3.580 | 212.0 | 11.45 | 0.093 |
| | 1.0 | 2950.0 | 0.878E-03 | 7.92 | 3.890 | 484.0 | 10.45 | 0.954 |
| | 10.0 | 2940.0 | 0.857E-03 | 7.86 | 3.890 | 494.0 | 10.43 | 1.000 |
| 0.090 | 0.1 | 3130.0 | 0.187E-02 | 10.20 | 3.400 | 212.0 | 11.34 | 0.067 |
| | 1.0 | 2810.0 | 0.635E-03 | 7.39 | 3.600 | 560.0 | 10.10 | 0.901 |
| | 10.0 | 2780.0 | 0.587E-03 | 7.26 | 3.580 | 591.0 | 10.03 | 0.999 |
| | 20.0 | 2780.0 | 0.587E-03 | 7.26 | 3.580 | 591.0 | 10.02 | 1.000 |
| 0.085 | 0.1 | 3090.0 | 0.172E-02 | 10.00 | 3.220 | 211.0 | 11.22 | 0.047 |
| | 1.0 | 2620.0 | 0.410E-03 | 6.86 | 3.210 | 658.0 | 9.68 | 0.753 |
| | 10.0 | 2390.0 | 0.246E-03 | 6.34 | 2.950 | 832.0 | 9.25 | 0.970 |
| | 20.0 | 2360.0 | 0.228E-03 | 6.28 | 2.910 | 854.0 | 9.19 | 0.996 |
| 0.080 | 0.1 | 3050.0 | 0.157E-02 | 9.85 | 3.030 | 210.0 | 11.09 | 0.032 |
| | 1.0 | 2360.0 | 0.242E-03 | 6.46 | 2.750 | 738.0 | 9.26 | 0.494 |
| | 10.0 | 1760.0 | 0.647E-04 | 5.99 | 2.400 | 919.0 | 8.77 | 0.971 |
| | 20.0 | 1730.0 | 0.597E-04 | 5.96 | 2.370 | 933.0 | 8.74 | 0.988 |
| 0.075 | 0.1 | 3010.0 | 0.141E-02 | 9.64 | 2.840 | 209.0 | 10.95 | 0.021 |
| | 1.0 | 2020.0 | 0.123E-03 | 6.29 | 2.370 | 742.0 | 8.99 | 0.331 |
| | 10.0 | 1100.0 | 0.821E-05 | 5.48 | 1.480 | 1110.0 | 7.79 | 0.276 |
| | 20.0 | 796.0 | 0.212E-05 | 5.32 | 1.150 | 1210.0 | 7.38 | 0.169 |
| 0.070 | 0.1 | 2890.0 | 0.106E-02 | 9.01 | 2.660 | 237.0 | 10.64 | 0.019 |
| | 1.0 | 1760.0 | 0.708E-04 | 6.26 | 2.090 | 698.0 | 8.84 | 0.196 |
| | 10.0 | 909.0 | 0.381E-05 | 5.48 | 1.200 | 1030.0 | 7.56 | 0.094 |
| | 20.0 | 668.0 | 0.107E-05 | 5.37 | 0.957 | 1090.0 | 7.25 | 0.054 |
| 0.060 | 0.1 | 2750.0 | 0.817E-03 | 8.75 | 2.220 | 219.0 | 10.36 | 0.005 |
| | 1.0 | 1540.0 | 0.420E-04 | 6.34 | 1.630 | 567.0 | 8.65 | 0.033 |
| | 10.0 | 749.0 | 0.186E-05 | 5.63 | 0.922 | 801.0 | 7.41 | 0.011 |
| | 20.0 | 568.0 | 0.598E-06 | 5.55 | 0.768 | 835.0 | 7.15 | 0.007 |
| 0.050 | 0.1 | 2560.0 | 0.575E-03 | 8.46 | 1.760 | 198.0 | 10.02 | 0.001 |
| | 1.0 | 1370.0 | 0.274E-04 | 6.49 | 1.240 | 433.0 | 8.47 | 0.003 |
| | 10.0 | 635.0 | 0.104E-05 | 5.85 | 0.709 | 584.0 | 7.32 | 0.001 |
| | 20.0 | 496.0 | 0.375E-06 | 5.77 | 0.608 | 606.0 | 7.09 | 0.001 |
| 0.040 | 0.1 | 2230.0 | 0.307E-03 | 8.13 | 1.290 | 174.0 | 9.58 | 0.000 |
| | 1.0 | 1170.0 | 0.156E-04 | 6.68 | 0.895 | 309.0 | 8.28 | 0.000 |
| | 10.0 | 536.0 | 0.578E-06 | 6.12 | 0.523 | 398.0 | 7.24 | 0.000 |
| | 20.0 | 427.0 | 0.227E-06 | 6.05 | 0.461 | 412.0 | 7.02 | 0.000 |
| 0.030 | 0.1 | 1740.0 | 0.113E-03 | 8.15 | 0.873 | 125.0 | 9.24 | 0.000 |
| | 1.0 | 948.0 | 0.728E-05 | 6.96 | 0.602 | 198.0 | 8.08 | 0.000 |
| | 10.0 | 442.0 | 0.297E-06 | 6.46 | 0.361 | 245.0 | 7.14 | 0.000 |
| | 20.0 | 356.0 | 0.122E-06 | 6.38 | 0.324 | 253.0 | 6.92 | 0.000 |

[a] H: $Y_\alpha = 0.22$; $\alpha = \infty$.

TABLE 4

MODEL B[a]

| Mass ($M_\odot$) | Age ($10^9$ yrs) | $T_e$(K) | Lum ($L_\odot$) | Rad ($10^9$ cm) | $T_c$ ($10^6$) | $\rho_c$ | S | $L_n/L$ |
|---|---|---|---|---|---|---|---|---|
| 0.200 | 10.0 | 3480.0 | 0.645E-02 | 15.30 | 6.000 | 146.0 | 13.25 | 1.000 |
| 0.150 | 10.0 | 3320.0 | 0.343E-02 | 12.30 | 5.290 | 210.0 | 12.37 | 1.000 |
| 0.125 | 0.1 | 3250.0 | 0.311E-02 | 12.30 | 4.370 | 176.0 | 12.20 | 0.235 |
| | 1.0 | 3210.0 | 0.220E-02 | 10.50 | 4.820 | 275.0 | 11.74 | 0.996 |
| | 10.0 | 3210.0 | 0.220E-02 | 10.50 | 4.820 | 276.0 | 11.73 | 1.000 |
| 0.110 | 0.1 | 3190.0 | 0.261E-02 | 11.70 | 3.940 | 178.0 | 11.94 | 0.129 |
| | 1.0 | 3130.0 | 0.155E-02 | 9.32 | 4.450 | 347.0 | 11.21 | 0.989 |
| | 10.0 | 3130.0 | 0.154E-02 | 9.31 | 4.450 | 349.0 | 11.21 | 1.000 |
| 0.100 | 0.1 | 3150.0 | 0.230E-02 | 11.20 | 3.640 | 180.0 | 11.74 | 0.079 |
| | 1.0 | 3010.0 | 0.110E-02 | 8.44 | 4.110 | 422.0 | 10.76 | 0.973 |
| | 10.0 | 3010.0 | 0.108E-02 | 8.41 | 4.120 | 427.0 | 10.75 | 1.000 |
| 0.095 | 0.1 | 3120.0 | 0.214E-02 | 11.00 | 3.480 | 181.0 | 11.63 | 0.060 |
| | 1.0 | 2920.0 | 0.861E-03 | 7.97 | 3.890 | 475.0 | 10.48 | 0.951 |
| | 10.0 | 2910.0 | 0.840E-03 | 7.91 | 3.890 | 486.0 | 10.45 | 1.000 |
| 0.090 | 0.1 | 3100.0 | 0.199E-02 | 10.80 | 3.320 | 182.0 | 11.51 | 0.045 |
| | 1.0 | 2800.0 | 0.631E-03 | 7.44 | 3.610 | 550.0 | 10.13 | 0.896 |
| | 10.0 | 2770.0 | 0.583E-03 | 7.30 | 3.590 | 581.0 | 10.05 | 1.000 |
| 0.085 | 0.1 | 3070.0 | 0.183E-02 | 10.50 | 3.150 | 183.0 | 11.38 | 0.032 |
| | 1.0 | 2620.0 | 0.416E-03 | 6.90 | 3.220 | 645.0 | 9.71 | 0.748 |
| | 10.0 | 2410.0 | 0.256E-03 | 6.39 | 2.980 | 812.0 | 9.29 | 0.973 |
| | 20.0 | 2380.0 | 0.240E-03 | 6.33 | 2.950 | 834.0 | 9.24 | 0.990 |
| 0.080 | 0.1 | 3030.0 | 0.167E-02 | 10.30 | 2.980 | 184.0 | 11.25 | 0.023 |
| | 1.0 | 2370.0 | 0.249E-03 | 6.50 | 2.780 | 723.0 | 9.30 | 0.496 |
| | 10.0 | 1770.0 | 0.660E-04 | 6.00 | 2.410 | 914.0 | 8.79 | 0.974 |
| | 20.0 | 1740.0 | 0.615E-04 | 5.98 | 2.380 | 926.0 | 8.76 | 0.990 |
| 0.075 | 0.1 | 3000.0 | 0.151E-02 | 10.00 | 2.800 | 185.0 | 11.10 | 0.015 |
| | 1.0 | 2050.0 | 0.131E-03 | 6.32 | 2.400 | 732.0 | 9.02 | 0.324 |
| | 10.0 | 1110.0 | 0.839E-05 | 5.48 | 1.490 | 1110.0 | 7.80 | 0.285 |
| | 20.0 | 787.0 | 0.203E-05 | 5.33 | 1.190 | 1200.0 | 7.42 | 0.226 |
| 0.070 | 0.1 | 2940.0 | 0.133E-02 | 9.78 | 2.610 | 185.0 | 10.94 | 0.010 |
| | 1.0 | 1800.0 | 0.772E-04 | 6.29 | 2.110 | 689.0 | 8.87 | 0.190 |
| | 10.0 | 898.0 | 0.365E-05 | 5.48 | 1.220 | 1030.0 | 7.57 | 0.106 |
| | 20.0 | 666.0 | 0.106E-05 | 5.38 | 0.985 | 1080.0 | 7.29 | 0.070 |
| 0.060 | 0.1 | 2790.0 | 0.980E-03 | 9.29 | 2.210 | 183.0 | 10.60 | 0.003 |
| | 1.0 | 1550.0 | 0.438E-04 | 6.37 | 1.650 | 561.0 | 8.67 | 0.034 |
| | 10.0 | 735.0 | 0.173E-05 | 5.64 | 0.936 | 798.0 | 7.43 | 0.013 |
| | 20.0 | 566.0 | 0.592E-06 | 5.56 | 0.783 | 830.0 | 7.19 | 0.008 |
| 0.050 | 0.1 | 2610.0 | 0.670E-03 | 8.81 | 1.780 | 175.0 | 10.20 | 0.001 |
| | 1.0 | 1370.0 | 0.281E-04 | 6.51 | 1.250 | 430.0 | 8.49 | 0.003 |
| | 10.0 | 630.0 | 0.101E-05 | 5.86 | 0.721 | 582.0 | 7.34 | 0.001 |
| | 20.0 | 495.0 | 0.375E-06 | 5.78 | 0.616 | 604.0 | 7.12 | 0.001 |
| 0.040 | 0.1 | 2290.0 | 0.358E-03 | 8.35 | 1.310 | 161.0 | 9.71 | 0.000 |
| | 1.0 | 1180.0 | 0.161E-04 | 6.70 | 0.902 | 308.0 | 8.29 | 0.000 |
| | 10.0 | 535.0 | 0.572E-06 | 6.13 | 0.530 | 397.0 | 7.26 | 0.000 |
| | 20.0 | 427.0 | 0.227E-06 | 6.05 | 0.464 | 411.0 | 7.03 | 0.000 |
| 0.030 | 0.1 | 1800.0 | 0.133E-03 | 8.26 | 0.887 | 120.0 | 9.31 | 0.000 |
| | 1.0 | 954.0 | 0.748E-05 | 6.97 | 0.606 | 197.0 | 8.09 | 0.000 |
| | 10.0 | 443.0 | 0.298E-06 | 6.46 | 0.362 | 245.0 | 7.14 | 0.000 |
| | 20.0 | 356.0 | 0.122E-06 | 6.38 | 0.324 | 253.0 | 6.92 | 0.000 |

[a] H: $Y_\alpha = 0.22$; $\alpha = 1.0$.

TABLE 5

MODEL C[a]

| Mass ($M_\odot$) | Age ($10^9$ yrs) | $T_e$(K) | Lum ($L_\odot$) | Rad ($10^9$ cm) | $T_c$ ($10^6$) | $\rho_c$ | S | $L_n/L$ |
|---|---|---|---|---|---|---|---|---|
| 0.200 | 10.0 | 3360.0 | 0.575E-02 | 15.60 | 5.930 | 140.0 | 13.29 | 1.000 |
| 0.150 | 10.0 | 3230.0 | 0.315E-02 | 12.40 | 5.250 | 203.0 | 12.41 | 1.000 |
| 0.125 | 0.1 | 3170.0 | 0.300E-02 | 12.60 | 4.290 | 161.0 | 12.29 | 0.196 |
| | 1.0 | 3160.0 | 0.209E-02 | 10.60 | 4.800 | 269.0 | 11.76 | 0.996 |
| | 10.0 | 3160.0 | 0.209E-02 | 10.60 | 4.800 | 270.0 | 11.76 | 1.000 |
| 0.110 | 0.1 | 3130.0 | 0.256E-02 | 12.00 | 3.870 | 164.0 | 12.03 | 0.106 |
| | 1.0 | 3090.0 | 0.149E-02 | 9.39 | 4.430 | 340.0 | 11.23 | 0.987 |
| | 10.0 | 3090.0 | 0.148E-02 | 9.37 | 4.440 | 342.0 | 11.23 | 1.000 |
| 0.100 | 0.1 | 3090.0 | 0.227E-02 | 11.60 | 3.580 | 165.0 | 11.83 | 0.065 |
| | 1.0 | 2980.0 | 0.106E-02 | 8.51 | 4.100 | 412.0 | 10.79 | 0.971 |
| | 10.0 | 2970.0 | 0.105E-02 | 8.47 | 4.110 | 417.0 | 10.77 | 1.000 |
| 0.095 | 0.1 | 3070.0 | 0.213E-02 | 11.30 | 3.420 | 166.0 | 11.72 | 0.050 |
| | 1.0 | 2890.0 | 0.841E-03 | 8.02 | 3.890 | 465.0 | 10.51 | 0.948 |
| | 10.0 | 2890.0 | 0.820E-03 | 7.96 | 3.890 | 476.0 | 10.48 | 1.000 |
| 0.090 | 0.1 | 3050.0 | 0.198E-02 | 11.10 | 3.270 | 167.0 | 11.60 | 0.037 |
| | 1.0 | 2780.0 | 0.625E-03 | 7.49 | 3.610 | 540.0 | 10.16 | 0.894 |
| | 10.0 | 2750.0 | 0.578E-03 | 7.34 | 3.590 | 571.0 | 10.08 | 0.999 |
| | 20.0 | 2750.0 | 0.578E-03 | 7.34 | 3.590 | 571.0 | 10.08 | 1.000 |
| 0.085 | 0.1 | 3030.0 | 0.183E-02 | 10.80 | 3.110 | 169.0 | 11.47 | 0.027 |
| | 1.0 | 2620.0 | 0.422E-03 | 6.95 | 3.240 | 634.0 | 9.74 | 0.741 |
| | 10.0 | 2410.0 | 0.259E-03 | 6.40 | 2.990 | 806.0 | 9.31 | 0.975 |
| | 20.0 | 2390.0 | 0.244E-03 | 6.35 | 2.960 | 827.0 | 9.26 | 0.991 |
| 0.080 | 0.1 | 3000.0 | 0.168E-02 | 10.60 | 2.940 | 170.0 | 11.33 | 0.019 |
| | 1.0 | 2390.0 | 0.257E-03 | 6.53 | 2.790 | 713.0 | 9.33 | 0.492 |
| | 10.0 | 1770.0 | 0.660E-04 | 6.00 | 2.410 | 914.0 | 8.79 | 0.974 |
| | 20.0 | 1740.0 | 0.615E-04 | 5.98 | 2.380 | 926.0 | 8.76 | 0.990 |
| 0.075 | 0.1 | 2960.0 | 0.151E-02 | 10.30 | 2.770 | 171.0 | 11.19 | 0.013 |
| | 1.0 | 2080.0 | 0.139E-03 | 6.34 | 2.410 | 726.0 | 9.04 | 0.313 |
| | 10.0 | 1110.0 | 0.844E-05 | 5.49 | 1.490 | 1110.0 | 7.80 | 0.286 |
| | 20.0 | 788.0 | 0.204E-05 | 5.33 | 1.190 | 1200.0 | 7.42 | 0.226 |
| 0.070 | 0.1 | 2910.0 | 0.134E-02 | 10.00 | 2.590 | 172.0 | 11.03 | 0.008 |
| | 1.0 | 1810.0 | 0.799E-04 | 6.30 | 2.120 | 685.0 | 8.88 | 0.186 |
| | 10.0 | 899.0 | 0.366E-05 | 5.48 | 1.220 | 1030.0 | 7.57 | 0.106 |
| | 20.0 | 666.0 | 0.106E-05 | 5.38 | 0.985 | 1080.0 | 7.29 | 0.070 |
| 0.060 | 0.1 | 2780.0 | 0.100E-02 | 9.49 | 2.200 | 172.0 | 10.68 | 0.003 |
| | 1.0 | 1560.0 | 0.445E-04 | 6.37 | 1.650 | 560.0 | 8.68 | 0.034 |
| | 10.0 | 735.0 | 0.173E-05 | 5.64 | 0.936 | 798.0 | 7.43 | 0.013 |
| | 20.0 | 566.0 | 0.592E-06 | 5.56 | 0.783 | 830.0 | 7.19 | 0.008 |
| 0.050 | 0.1 | 2610.0 | 0.695E-03 | 8.95 | 1.780 | 167.0 | 10.26 | 0.001 |
| | 1.0 | 1380.0 | 0.283E-04 | 6.51 | 1.250 | 429.0 | 8.50 | 0.003 |
| | 10.0 | 630.0 | 0.101E-05 | 5.86 | 0.722 | 582.0 | 7.34 | 0.001 |
| | 20.0 | 495.0 | 0.375E-06 | 5.78 | 0.616 | 604.0 | 7.12 | 0.001 |
| 0.040 | 0.1 | 2310.0 | 0.373E-03 | 8.42 | 1.320 | 157.0 | 9.75 | 0.000 |
| | 1.0 | 1180.0 | 0.162E-04 | 6.70 | 0.903 | 307.0 | 8.30 | 0.000 |
| | 10.0 | 535.0 | 0.572E-06 | 6.13 | 0.530 | 397.0 | 7.26 | 0.000 |
| | 20.0 | 427.0 | 0.227E-06 | 6.05 | 0.464 | 411.0 | 7.03 | 0.000 |
| 0.030 | 0.1 | 1810.0 | 0.137E-03 | 8.28 | 0.889 | 119.0 | 9.33 | 0.000 |
| | 1.0 | 954.0 | 0.750E-05 | 6.97 | 0.606 | 197.0 | 8.09 | 0.000 |
| | 10.0 | 443.0 | 0.298E-06 | 6.46 | 0.362 | 245.0 | 7.14 | 0.000 |
| | 20.0 | 356.0 | 0.122E-06 | 6.38 | 0.324 | 253.0 | 6.92 | 0.000 |

[a] H: $Y_\alpha = 0.22$; $\alpha = 0.5$.

TABLE 6

MODEL D[a]

| Mass ($M_\odot$) | Age ($10^9$ yrs) | $T_e$(K) | Lum ($L_\odot$) | Rad ($10^9$ cm) | $T_c$ ($10^6$) | $\rho_c$ | S | $L_n/L$ |
|---|---|---|---|---|---|---|---|---|
| 0.200 | 10.0 | 3010.0 | 0.402E-02 | 16.30 | 5.710 | 123.0 | 13.41 | 1.000 |
| 0.150 | 10.0 | 2940.0 | 0.233E-02 | 12.90 | 5.100 | 180.0 | 12.52 | 1.000 |
| 0.125 | 0.1 | 2880.0 | 0.246E-02 | 13.80 | 4.010 | 123.0 | 12.56 | 0.115 |
| | 1.0 | 2880.0 | 0.157E-02 | 11.10 | 4.670 | 237.0 | 11.89 | 0.992 |
| | 10.0 | 2880.0 | 0.157E-02 | 11.10 | 4.680 | 239.0 | 11.89 | 1.000 |
| 0.110 | 0.1 | 2850.0 | 0.217E-02 | 13.30 | 3.600 | 120.0 | 12.34 | 0.055 |
| | 1.0 | 2820.0 | 0.114E-02 | 9.82 | 4.340 | 297.0 | 11.38 | 0.978 |
| | 10.0 | 2820.0 | 0.113E-02 | 9.79 | 4.350 | 300.0 | 11.38 | 1.000 |
| 0.100 | 0.1 | 2820.0 | 0.196E-02 | 12.90 | 3.330 | 118.0 | 12.17 | 0.032 |
| | 1.0 | 2760.0 | 0.858E-03 | 8.89 | 4.060 | 361.0 | 10.95 | 0.955 |
| | 10.0 | 2760.0 | 0.845E-03 | 8.84 | 4.060 | 368.0 | 10.93 | 1.000 |
| 0.095 | 0.1 | 2800.0 | 0.186E-02 | 12.70 | 3.190 | 118.0 | 12.07 | 0.024 |
| | 1.0 | 2720.0 | 0.715E-03 | 8.39 | 3.870 | 408.0 | 10.68 | 0.929 |
| | 10.0 | 2710.0 | 0.695E-03 | 8.30 | 3.880 | 421.0 | 10.64 | 1.000 |
| 0.090 | 0.1 | 2790.0 | 0.174E-02 | 12.50 | 3.050 | 118.0 | 11.97 | 0.017 |
| | 1.0 | 2660.0 | 0.573E-03 | 7.85 | 3.640 | 469.0 | 10.36 | 0.864 |
| | 10.0 | 2640.0 | 0.530E-03 | 7.65 | 3.630 | 505.0 | 10.26 | 0.999 |
| | 20.0 | 2640.0 | 0.530E-03 | 7.65 | 3.630 | 505.0 | 10.25 | 1.000 |
| 0.085 | 0.1 | 2770.0 | 0.163E-02 | 12.20 | 2.900 | 118.0 | 11.85 | 0.012 |
| | 1.0 | 2560.0 | 0.428E-03 | 7.29 | 3.320 | 549.0 | 9.97 | 0.727 |
| | 10.0 | 2450.0 | 0.305E-03 | 6.74 | 3.170 | 692.0 | 9.59 | 0.985 |
| | 20.0 | 2440.0 | 0.298E-03 | 6.72 | 3.150 | 701.0 | 9.57 | 0.998 |
| 0.080 | 0.1 | 2750.0 | 0.151E-02 | 11.90 | 2.760 | 118.0 | 11.73 | 0.009 |
| | 1.0 | 2420.0 | 0.299E-03 | 6.82 | 2.920 | 627.0 | 9.56 | 0.493 |
| | 10.0 | 1830.0 | 0.770E-04 | 6.08 | 2.480 | 880.0 | 8.88 | 0.968 |
| | 20.0 | 1800.0 | 0.715E-04 | 6.06 | 2.460 | 891.0 | 8.85 | 0.996 |
| 0.075 | 0.1 | 2730.0 | 0.139E-02 | 11.60 | 2.610 | 119.0 | 11.59 | 0.006 |
| | 1.0 | 2130.0 | 0.165E-03 | 6.53 | 2.530 | 664.0 | 9.23 | 0.328 |
| | 10.0 | 1180.0 | 0.109E-04 | 5.52 | 1.550 | 1090.0 | 7.88 | 0.289 |
| | 20.0 | 805.0 | 0.222E-05 | 5.33 | 1.180 | 1210.0 | 7.41 | 0.195 |
| 0.070 | 0.1 | 2700.0 | 0.127E-02 | 11.30 | 2.460 | 120.0 | 11.44 | 0.004 |
| | 1.0 | 1890.0 | 0.993E-04 | 6.46 | 2.220 | 637.0 | 9.05 | 0.191 |
| | 10.0 | 936.0 | 0.432E-05 | 5.50 | 1.240 | 1020.0 | 7.61 | 0.105 |
| | 20.0 | 678.0 | 0.114E-05 | 5.38 | 0.988 | 1080.0 | 7.29 | 0.067 |
| 0.060 | 0.1 | 2640.0 | 0.102E-02 | 10.60 | 2.130 | 122.0 | 11.09 | 0.001 |
| | 1.0 | 1610.0 | 0.530E-04 | 6.47 | 1.710 | 534.0 | 8.79 | 0.035 |
| | 10.0 | 760.0 | 0.200E-05 | 5.67 | 0.980 | 787.0 | 7.50 | 0.017 |
| | 20.0 | 581.0 | 0.659E-06 | 5.58 | 0.805 | 823.0 | 7.25 | 0.010 |
| 0.050 | 0.1 | 2550.0 | 0.767E-03 | 9.88 | 1.770 | 125.0 | 10.66 | 0.000 |
| | 1.0 | 1400.0 | 0.312E-04 | 6.58 | 1.300 | 415.0 | 8.59 | 0.004 |
| | 10.0 | 651.0 | 0.117E-05 | 5.91 | 0.786 | 568.0 | 7.47 | 0.002 |
| | 20.0 | 512.0 | 0.434E-06 | 5.82 | 0.657 | 593.0 | 7.24 | 0.001 |
| 0.040 | 0.1 | 2370.0 | 0.464E-03 | 8.89 | 1.350 | 133.0 | 10.00 | 0.000 |
| | 1.0 | 1160.0 | 0.153E-04 | 6.76 | 0.932 | 299.0 | 8.38 | 0.000 |
| | 10.0 | 552.0 | 0.668E-06 | 6.21 | 0.612 | 382.0 | 7.46 | 0.000 |
| | 20.0 | 444.0 | 0.272E-06 | 6.12 | 0.519 | 398.0 | 7.23 | 0.000 |
| 0.030 | 0.1 | 1850.0 | 0.156E-03 | 8.45 | 0.909 | 112.0 | 9.44 | 0.000 |
| | 1.0 | 904.0 | 0.620E-05 | 7.07 | 0.639 | 189.0 | 8.23 | 0.000 |
| | 10.0 | 452.0 | 0.338E-06 | 6.58 | 0.445 | 232.0 | 7.44 | 0.000 |
| | 20.0 | 371.0 | 0.149E-06 | 6.49 | 0.385 | 242.0 | 7.22 | 0.000 |

[a] H: $Y_\alpha = 0.22$; $\alpha = 0.1$.

TABLE 7

MODEL E[a]

| Mass ($M_\odot$) | Age ($10^9$ yrs) | $T_e$(K) | Lum ($L_\odot$) | Rad ($10^9$ cm) | $T_c$ ($10^6$) | $\rho_c$ | S | $L_n/L$ |
|---|---|---|---|---|---|---|---|---|
| 0.150 | 10.0 | 3640.0 | 0.458E-02 | 11.80 | 5.440 | 236.0 | 12.26 | 1.000 |
| 0.135 | 0.1 | 3600.0 | 0.437E-02 | 11.80 | 4.870 | 213.0 | 12.16 | 0.434 |
| | 1.0 | 3580.0 | 0.358E-02 | 10.80 | 5.160 | 276.0 | 11.89 | 0.999 |
| | 10.0 | 3580.0 | 0.358E-02 | 10.80 | 5.160 | 277.0 | 11.89 | 1.000 |
| 0.125 | 0.1 | 3570.0 | 0.385E-02 | 11.30 | 4.610 | 223.0 | 11.96 | 0.344 |
| | 1.0 | 3530.0 | 0.295E-02 | 10.10 | 4.940 | 314.0 | 11.60 | 0.995 |
| | 10.0 | 3530.0 | 0.295E-02 | 10.10 | 4.940 | 314.0 | 11.59 | 1.000 |
| 0.110 | 0.1 | 3500.0 | 0.315E-02 | 10.60 | 4.170 | 235.0 | 11.64 | 0.210 |
| | 1.0 | 3420.0 | 0.202E-02 | 8.90 | 4.530 | 399.0 | 11.05 | 0.992 |
| | 10.0 | 3420.0 | 0.201E-02 | 8.89 | 4.530 | 400.0 | 11.04 | 1.000 |
| 0.100 | 0.1 | 3450.0 | 0.271E-02 | 10.20 | 3.840 | 243.0 | 11.41 | 0.136 |
| | 1.0 | 3290.0 | 0.139E-02 | 7.99 | 4.150 | 498.0 | 10.55 | 0.975 |
| | 10.0 | 3290.0 | 0.137E-02 | 7.95 | 4.150 | 504.0 | 10.53 | 1.000 |
| 0.095 | 0.1 | 3420.0 | 0.249E-02 | 9.92 | 3.670 | 247.0 | 11.28 | 0.106 |
| | 1.0 | 3180.0 | 0.105E-02 | 7.44 | 3.870 | 581.0 | 10.20 | 0.951 |
| | 10.0 | 3170.0 | 0.102E-02 | 7.38 | 3.860 | 596.0 | 10.16 | 1.000 |
| 0.090 | 0.1 | 3380.0 | 0.228E-02 | 9.68 | 3.490 | 251.0 | 11.15 | 0.080 |
| | 1.0 | 3000.0 | 0.692E-03 | 6.79 | 3.450 | 722.0 | 9.70 | 0.858 |
| | 10.0 | 2890.0 | 0.539E-03 | 6.43 | 3.290 | 846.0 | 9.42 | 0.977 |
| | 20.0 | 2870.0 | 0.513E-03 | 6.37 | 3.250 | 870.0 | 9.37 | 0.991 |
| 0.085 | 0.1 | 3340.0 | 0.207E-02 | 9.44 | 3.300 | 254.0 | 11.00 | 0.058 |
| | 1.0 | 2720.0 | 0.381E-03 | 6.12 | 2.800 | 920.0 | 9.03 | 0.497 |
| | 10.0 | 944.0 | 0.362E-05 | 4.95 | 0.840 | 1710.0 | 6.55 | 0.016 |
| | 20.0 | 745.0 | 0.137E-05 | 4.88 | 0.672 | 1780.0 | 6.13 | 0.007 |
| 0.080 | 0.1 | 3290.0 | 0.186E-02 | 9.21 | 3.100 | 257.0 | 10.85 | 0.040 |
| | 1.0 | 2460.0 | 0.226E-03 | 5.75 | 2.140 | 1040.0 | 8.45 | 0.148 |
| | 10.0 | 876.0 | 0.275E-05 | 5.01 | 0.734 | 1550.0 | 6.42 | 0.005 |
| | 20.0 | 700.0 | 0.109E-05 | 4.94 | 0.593 | 1610.0 | 6.02 | 0.002 |
| 0.075 | 0.1 | 3240.0 | 0.165E-02 | 8.97 | 2.890 | 259.0 | 10.69 | 0.026 |
| | 1.0 | 2190.0 | 0.136E-03 | 5.62 | 1.700 | 1030.0 | 8.07 | 0.043 |
| | 10.0 | 827.0 | 0.224E-05 | 5.07 | 0.647 | 1390.0 | 6.32 | 0.002 |
| | 20.0 | 662.0 | 0.897E-06 | 5.01 | 0.524 | 1440.0 | 5.92 | 0.001 |
| 0.070 | 0.1 | 3180.0 | 0.146E-02 | 8.74 | 2.670 | 260.0 | 10.52 | 0.016 |
| | 1.0 | 1950.0 | 0.851E-04 | 5.60 | 1.400 | 969.0 | 7.84 | 0.013 |
| | 10.0 | 782.0 | 0.184E-05 | 5.14 | 0.569 | 1240.0 | 6.22 | 0.000 |
| | 20.0 | 625.0 | 0.733E-06 | 5.08 | 0.461 | 1270.0 | 5.83 | 0.000 |
| 0.060 | 0.1 | 3030.0 | 0.107E-02 | 8.27 | 2.200 | 258.0 | 10.12 | 0.004 |
| | 1.0 | 1600.0 | 0.394E-04 | 5.67 | 0.985 | 785.0 | 7.51 | 0.001 |
| | 10.0 | 690.0 | 0.118E-05 | 5.30 | 0.429 | 950.0 | 6.01 | 0.000 |
| | 20.0 | 550.0 | 0.471E-06 | 5.25 | 0.349 | 977.0 | 5.62 | 0.000 |
| 0.050 | 0.1 | 2820.0 | 0.723E-03 | 7.83 | 1.690 | 249.0 | 9.65 | 0.001 |
| | 1.0 | 1340.0 | 0.202E-04 | 5.81 | 0.646 | 595.0 | 7.21 | 0.000 |
| | 10.0 | 595.0 | 0.703E-06 | 5.49 | 0.310 | 697.0 | 5.76 | 0.000 |
| | 20.0 | 474.0 | 0.279E-06 | 5.45 | 0.253 | 714.0 | 5.38 | 0.000 |
| 0.040 | 0.1 | 2530.0 | 0.421E-03 | 7.40 | 1.150 | 229.0 | 9.04 | 0.000 |
| | 1.0 | 1100.0 | 0.972E-05 | 6.00 | 0.429 | 420.0 | 6.87 | 0.000 |
| | 10.0 | 497.0 | 0.372E-06 | 5.73 | 0.212 | 479.0 | 5.48 | 0.000 |
| | 20.0 | 397.0 | 0.150E-06 | 5.69 | 0.175 | 489.0 | 5.12 | 0.000 |
| 0.030 | 0.1 | 2050.0 | 0.167E-03 | 7.15 | 0.666 | 183.0 | 8.33 | 0.000 |
| | 1.0 | 878.0 | 0.432E-05 | 6.25 | 0.260 | 268.0 | 6.46 | 0.000 |
| | 10.0 | 397.0 | 0.168E-06 | 6.02 | 0.133 | 297.0 | 5.15 | 0.000 |
| | 20.0 | 320.0 | 0.701E-07 | 5.99 | 0.111 | 302.0 | 4.80 | 0.000 |

[a] L: $Y_\alpha = 0.22; \alpha = 0.5$.

TABLE 8

MODEL F[a]

| Mass ($M_\odot$) | Age ($10^9$ yrs) | $T_e$(K) | Lum ($L_\odot$) | Rad ($10^9$ cm) | $T_c$ ($10^6$) | $\rho_c$ | S | $L_n/L$ |
|---|---|---|---|---|---|---|---|---|
| 0.200 | 10.0 | 3540.0 | 0.681E-02 | 15.20 | 6.040 | 149.0 | 13.23 | 1.000 |
| 0.150 | 10.0 | 3410.0 | 0.372E-02 | 12.20 | 5.340 | 217.0 | 12.34 | 1.000 |
| 0.125 | 0.1 | 3320.0 | 0.303E-02 | 11.60 | 4.540 | 208.0 | 12.03 | 0.368 |
| | 1.0 | 3280.0 | 0.234E-02 | 10.40 | 4.840 | 283.0 | 11.71 | 0.996 |
| | 10.0 | 3280.0 | 0.234E-02 | 10.40 | 4.850 | 284.0 | 11.70 | 1.000 |
| 0.110 | 0.1 | 3240.0 | 0.251E-02 | 11.00 | 4.080 | 210.0 | 11.76 | 0.201 |
| | 1.0 | 3140.0 | 0.156E-02 | 9.31 | 4.450 | 348.0 | 11.21 | 0.990 |
| | 10.0 | 3140.0 | 0.155E-02 | 9.30 | 4.450 | 350.0 | 11.20 | 1.000 |
| 0.100 | 0.1 | 3180.0 | 0.217E-02 | 10.70 | 3.750 | 210.0 | 11.57 | 0.121 |
| | 1.0 | 2980.0 | 0.106E-02 | 8.49 | 4.110 | 414.0 | 10.78 | 0.977 |
| | 10.0 | 2980.0 | 0.105E-02 | 8.47 | 4.110 | 418.0 | 10.77 | 1.000 |
| 0.095 | 0.1 | 3140.0 | 0.200E-02 | 10.50 | 3.570 | 209.0 | 11.47 | 0.091 |
| | 1.0 | 2870.0 | 0.822E-03 | 8.05 | 3.890 | 460.0 | 10.52 | 0.957 |
| | 10.0 | 2860.0 | 0.804E-03 | 8.00 | 3.890 | 468.0 | 10.50 | 1.000 |
| 0.090 | 0.1 | 3100.0 | 0.183E-02 | 10.30 | 3.390 | 208.0 | 11.36 | 0.066 |
| | 1.0 | 2730.0 | 0.593E-03 | 7.58 | 3.620 | 520.0 | 10.21 | 0.916 |
| | 10.0 | 2700.0 | 0.558E-03 | 7.49 | 3.610 | 540.0 | 10.16 | 1.000 |
| 0.085 | 0.1 | 3060.0 | 0.167E-02 | 10.10 | 3.210 | 206.0 | 11.25 | 0.046 |
| | 1.0 | 2550.0 | 0.396E-03 | 7.11 | 3.280 | 592.0 | 9.85 | 0.795 |
| | 10.0 | 2440.0 | 0.307E-03 | 6.82 | 3.200 | 668.0 | 9.65 | 0.997 |
| | 20.0 | 2440.0 | 0.306E-03 | 6.82 | 3.200 | 669.0 | 9.65 | 1.000 |
| 0.080 | 0.1 | 3010.0 | 0.150E-02 | 9.94 | 3.020 | 204.0 | 11.13 | 0.032 |
| | 1.0 | 2340.0 | 0.252E-03 | 6.71 | 2.880 | 657.0 | 9.48 | 0.559 |
| | 10.0 | 1770.0 | 0.651E-04 | 5.99 | 2.400 | 918.0 | 8.78 | 0.969 |
| | 20.0 | 1730.0 | 0.598E-04 | 5.96 | 2.370 | 932.0 | 8.74 | 0.988 |
| 0.075 | 0.1 | 2940.0 | 0.133E-02 | 9.76 | 2.830 | 201.0 | 11.00 | 0.021 |
| | 1.0 | 2150.0 | 0.165E-03 | 6.44 | 2.470 | 692.0 | 9.14 | 0.299 |
| | 10.0 | 1110.0 | 0.852E-05 | 5.48 | 1.490 | 1110.0 | 7.80 | 0.280 |
| | 20.0 | 801.0 | 0.217E-05 | 5.32 | 1.160 | 1210.0 | 7.38 | 0.171 |
| 0.070 | 0.1 | 2880.0 | 0.117E-02 | 9.58 | 2.630 | 198.0 | 10.86 | 0.013 |
| | 1.0 | 1880.0 | 0.935E-04 | 6.34 | 2.140 | 673.0 | 8.93 | 0.171 |
| | 10.0 | 915.0 | 0.391E-05 | 5.48 | 1.210 | 1030.0 | 7.56 | 0.095 |
| | 20.0 | 670.0 | 0.108E-05 | 5.37 | 0.958 | 1090.0 | 7.25 | 0.054 |
| 0.060 | 0.1 | 2710.0 | 0.852E-03 | 9.23 | 2.210 | 187.0 | 10.57 | 0.004 |
| | 1.0 | 1580.0 | 0.468E-04 | 6.39 | 1.660 | 556.0 | 8.70 | 0.033 |
| | 10.0 | 753.0 | 0.190E-05 | 5.63 | 0.925 | 800.0 | 7.41 | 0.011 |
| | 20.0 | 569.0 | 0.602E-06 | 5.55 | 0.769 | 835.0 | 7.16 | 0.007 |
| 0.050 | 0.1 | 2500.0 | 0.577E-03 | 8.89 | 1.780 | 171.0 | 10.24 | 0.001 |
| | 1.0 | 1380.0 | 0.289E-04 | 6.51 | 1.260 | 428.0 | 8.50 | 0.003 |
| | 10.0 | 637.0 | 0.105E-05 | 5.85 | 0.711 | 584.0 | 7.33 | 0.001 |
| | 20.0 | 496.0 | 0.376E-06 | 5.77 | 0.608 | 606.0 | 7.09 | 0.001 |
| 0.040 | 0.1 | 2280.0 | 0.367E-03 | 8.52 | 1.330 | 151.0 | 9.81 | 0.000 |
| | 1.0 | 1180.0 | 0.162E-04 | 6.69 | 0.901 | 308.0 | 8.29 | 0.000 |
| | 10.0 | 537.0 | 0.580E-06 | 6.12 | 0.524 | 398.0 | 7.24 | 0.000 |
| | 20.0 | 428.0 | 0.228E-06 | 6.05 | 0.461 | 412.0 | 7.02 | 0.000 |
| 0.030 | 0.1 | 1840.0 | 0.147E-03 | 8.28 | 0.890 | 119.0 | 9.33 | 0.000 |
| | 1.0 | 952.0 | 0.742E-05 | 6.96 | 0.604 | 198.0 | 8.08 | 0.000 |
| | 10.0 | 442.0 | 0.298E-06 | 6.46 | 0.362 | 245.0 | 7.14 | 0.000 |
| | 20.0 | 356.0 | 0.122E-06 | 6.38 | 0.324 | 253.0 | 6.92 | 0.000 |

[a] ALEX83: $Y_\alpha = 0.22; \alpha = \infty$.

TABLE 9

MODEL G[a]

| Mass ($M_\odot$) | Age ($10^9$ yrs) | $T_e$(K) | Lum ($L_\odot$) | Rad ($10^9$ cm) | $T_c$ ($10^6$) | $\rho_c$ | S | $L_n/L$ |
|---|---|---|---|---|---|---|---|---|
| 0.200 | 10.0 | 3500.0 | 0.666E-02 | 15.40 | 6.140 | 144.0 | 13.07 | 1.000 |
| 0.150 | 10.0 | 3340.0 | 0.358E-02 | 12.40 | 5.420 | 206.0 | 12.22 | 1.000 |
| 0.125 | 0.1 | 3260.0 | 0.302E-02 | 12.00 | 4.580 | 188.0 | 11.96 | 0.323 |
| | 1.0 | 3230.0 | 0.230E-02 | 10.70 | 4.950 | 267.0 | 11.61 | 0.997 |
| | 10.0 | 3230.0 | 0.230E-02 | 10.70 | 4.950 | 267.0 | 11.61 | 1.000 |
| 0.110 | 0.1 | 3200.0 | 0.253E-02 | 11.40 | 4.130 | 190.0 | 11.71 | 0.178 |
| | 1.0 | 3150.0 | 0.164E-02 | 9.47 | 4.590 | 332.0 | 11.12 | 0.990 |
| | 10.0 | 3150.0 | 0.164E-02 | 9.45 | 4.590 | 334.0 | 11.12 | 1.000 |
| 0.100 | 0.1 | 3160.0 | 0.224E-02 | 11.00 | 3.810 | 191.0 | 11.52 | 0.109 |
| | 1.0 | 3060.0 | 0.120E-02 | 8.59 | 4.270 | 401.0 | 10.70 | 0.982 |
| | 10.0 | 3060.0 | 0.120E-02 | 8.57 | 4.280 | 404.0 | 10.69 | 1.000 |
| 0.095 | 0.1 | 3130.0 | 0.209E-02 | 10.80 | 3.640 | 192.0 | 11.41 | 0.083 |
| | 1.0 | 2980.0 | 0.971E-03 | 8.14 | 4.070 | 447.0 | 10.45 | 0.968 |
| | 10.0 | 2970.0 | 0.957E-03 | 8.10 | 4.080 | 453.0 | 10.43 | 1.000 |
| 0.090 | 0.1 | 3110.0 | 0.194E-02 | 10.60 | 3.470 | 192.0 | 11.30 | 0.061 |
| | 1.0 | 2870.0 | 0.740E-03 | 7.63 | 3.820 | 510.0 | 10.15 | 0.938 |
| | 10.0 | 2860.0 | 0.714E-03 | 7.56 | 3.820 | 525.0 | 10.11 | 1.000 |
| 0.085 | 0.1 | 3080.0 | 0.179E-02 | 10.40 | 3.290 | 193.0 | 11.18 | 0.044 |
| | 1.0 | 2720.0 | 0.513E-03 | 7.09 | 3.490 | 597.0 | 9.77 | 0.858 |
| | 10.0 | 2670.0 | 0.447E-03 | 6.88 | 3.440 | 653.0 | 9.63 | 0.997 |
| | 20.0 | 2670.0 | 0.446E-03 | 6.88 | 3.440 | 654.0 | 9.63 | 1.000 |
| 0.080 | 0.1 | 3050.0 | 0.164E-02 | 10.10 | 3.110 | 193.0 | 11.05 | 0.031 |
| | 1.0 | 2500.0 | 0.318E-03 | 6.59 | 3.050 | 697.0 | 9.33 | 0.650 |
| | 10.0 | 2100.0 | 0.134E-03 | 6.05 | 2.730 | 894.0 | 8.85 | 0.997 |
| | 20.0 | 2100.0 | 0.133E-03 | 6.05 | 2.720 | 895.0 | 8.85 | 1.000 |
| 0.075 | 0.1 | 3010.0 | 0.149E-02 | 9.89 | 2.930 | 194.0 | 10.91 | 0.021 |
| | 1.0 | 2200.0 | 0.173E-03 | 6.28 | 2.610 | 748.0 | 8.97 | 0.418 |
| | 10.0 | 1460.0 | 0.264E-04 | 5.62 | 1.990 | 1040.0 | 8.17 | 0.650 |
| | 20.0 | 1080.0 | 0.721E-05 | 5.32 | 1.540 | 1220.0 | 7.62 | 0.447 |
| 0.070 | 0.1 | 2960.0 | 0.132E-02 | 9.65 | 2.730 | 194.0 | 10.76 | 0.013 |
| | 1.0 | 1890.0 | 0.910E-04 | 6.19 | 2.270 | 723.0 | 8.77 | 0.267 |
| | 10.0 | 988.0 | 0.514E-05 | 5.38 | 1.350 | 1090.0 | 7.53 | 0.181 |
| | 20.0 | 715.0 | 0.135E-05 | 5.27 | 1.110 | 1160.0 | 7.23 | 0.155 |
| 0.060 | 0.1 | 2820.0 | 0.983E-03 | 9.16 | 2.320 | 191.0 | 10.43 | 0.005 |
| | 1.0 | 1590.0 | 0.460E-04 | 6.24 | 1.760 | 597.0 | 8.55 | 0.053 |
| | 10.0 | 761.0 | 0.190E-05 | 5.51 | 1.010 | 859.0 | 7.33 | 0.024 |
| | 20.0 | 584.0 | 0.639E-06 | 5.43 | 0.834 | 895.0 | 7.09 | 0.015 |
| 0.050 | 0.1 | 2630.0 | 0.678E-03 | 8.70 | 1.870 | 183.0 | 10.05 | 0.001 |
| | 1.0 | 1400.0 | 0.290E-04 | 6.37 | 1.340 | 458.0 | 8.37 | 0.005 |
| | 10.0 | 645.0 | 0.105E-05 | 5.72 | 0.775 | 627.0 | 7.24 | 0.002 |
| | 20.0 | 508.0 | 0.394E-06 | 5.64 | 0.655 | 651.0 | 7.02 | 0.001 |
| 0.040 | 0.1 | 2340.0 | 0.379E-03 | 8.26 | 1.390 | 166.0 | 9.59 | 0.000 |
| | 1.0 | 1210.0 | 0.169E-04 | 6.56 | 0.963 | 328.0 | 8.18 | 0.000 |
| | 10.0 | 548.0 | 0.600E-06 | 5.98 | 0.572 | 428.0 | 7.15 | 0.000 |
| | 20.0 | 436.0 | 0.236E-06 | 5.91 | 0.493 | 443.0 | 6.93 | 0.000 |
| 0.030 | 0.1 | 1850.0 | 0.143E-03 | 8.12 | 0.940 | 127.0 | 9.18 | 0.000 |
| | 1.0 | 975.0 | 0.781E-05 | 6.82 | 0.645 | 211.0 | 7.97 | 0.000 |
| | 10.0 | 452.0 | 0.309E-06 | 6.31 | 0.389 | 263.0 | 7.05 | 0.000 |
| | 20.0 | 364.0 | 0.127E-06 | 6.23 | 0.344 | 272.0 | 6.82 | 0.000 |

[a] H: $Y_\alpha = 0.25$; $\alpha = 1.0$.

## III. RESULTS

Useful compilations of numerical data derived for models A through G are rendered in Tables 3–9. For each model, 15 "stars" with masses (mass) 0.03, 0.04, 0.05, 0.06, 0.07, 0.075, 0.08, 0.085, 0.09, 0.095, 0.1, 0.11, 0.125, 0.15, and 0.2 $M_\odot$ were evolved 20 Gyr from extended initial structures ($R_{\rm initial} \gtrsim 2R_{\rm final}$, $T_c^i < 5 \times 10^5$ K). The tables give for various ages ($t = 10^8$, $10^9$, $10^{10}$, and $2 \times 10^{10}$ yr) the effective surface temperature ($T_e$ in K), the luminosity ($L$) in solar units ($L_\odot = 3.826 \times 10^{33}$ ergs s$^{-1}$), the radius ($R$, in units of $10^9$ cm), the central temperature ($T_c$, in units of $10^6$ K), the central density ($\rho_c$, in cgs), the entropy in the convective zone ($S$, per baryon per Boltzmann's constant), and the ratio ($L_n/L$) of the nuclear luminosity to the total luminosity. If $L_n/L = 1.0$ was achieved early in the object's life, only the $t = 10^{10}$ yr quantities are shown, and if the quantities at $2 \times 10^{10}$ yr were the same as those at $10^{10}$ yr, they are not repeated under the former.

Tables 3–9 contain our results for the evolution of brown dwarfs and VLMs for various mixing-length parameters ($\alpha$), helium fractions, and opacity models. Rather than describe the numbers, trends, and conclusions concerning the VLM/BD continuum and the edge of the hydrogen main sequence by referring directly only to these tables, we illustrate our results with the following figures. However, since the tables and figures complement one another, as would be expected of digital and analog representations of the same phenomena, the reader is encouraged periodically to refer back to the tables during the discussion below.

### a) Luminosity

Figure 5 depicts the luminosity ($L$) versus mass for models A–E and model G at age $10^{10}$ yr, roughly the age of the Galactic disc. The bolometric magnitude [$M_{\rm bol}(\odot) = 4.70$] corresponding to $L$ is given on the alternate ordinate. As Table 2 indicates, models A–D have the same helium fraction and opacities, but different mixing-length parameters, $\alpha$ ($= \infty$, 1.0, 0.5, 0.1, respectively). Model G differs from model B (high-opacity [H], $\alpha = 1.0$ $Y_\alpha = 0.22$) only in its larger helium fraction ($Y_\alpha =$

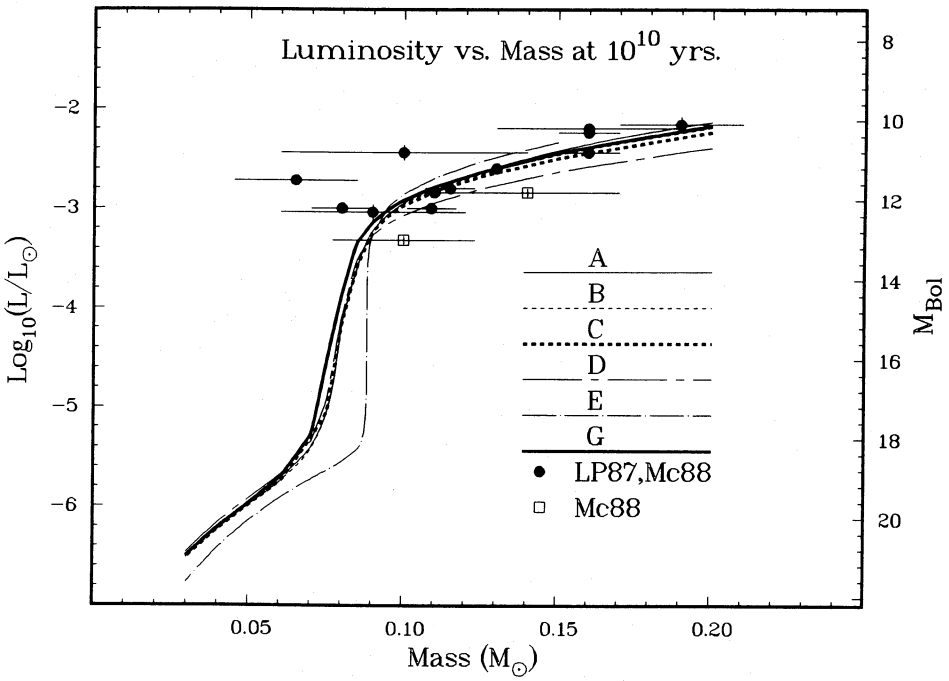


FIG. 5.—Luminosity and $M_{bol}[M_{bol}(\odot) = 4.70]$ vs. mass between 0.03 $M_\odot$ and 0.2 $M_\odot$ for models A–E and model G at ages of $10^{10}$ yr. Superposed are the data from Table 1 when both mass and luminosity have been obtained (LP87, Mc88). A few of the LP87 data points have been modified by Mc88. The brown dwarf branch is in the lower left, and the VLM branch is in the upper right.

0.25). The data (Table 1) from Liebert and Probst (1987), as modified by McCarthy *et al.* (1988*b*), and from McCarthy *et al.* (1988*b*, hereafter Mc88), with mass error bars and statistical luminosity error bars, are superposed on the plot for comparison with theory. The data range only between 10 and 12 mag bolometric and a factor of approximately 3 in mass. The mass error bars should not be taken lightly, and a systematic bias in the data to lower masses is a distinct possibility.

Figure 5 clearly shows the transition from brown dwarfs (on the left) to VLMs (on the right). These two families are connected by a steep transition region around 0.07–0.09 $M_\odot$, covering a full two orders of magnitude in luminosity in a very narrow mass range ($\sim$0.02 $M_\odot$). This $L \propto M^{20}$ ramp between BDs and VLMs is characteristic of the tip of the hydrogen main sequence, but between 0.1 and 0.2 $M_\odot$, $L$'s dependence on $M$ slows to a relatively sluggish $L \propto M^2$. Since their cooling could not be stabilized by nuclear burning, the brown dwarfs ($<$0.07 $M_\odot$) are a dim $10^{-6}$ $L_\odot$ after $10^{10}$ yr. On the other hand, the 0.15–0.2 $M_\odot$ stars that did land on the main sequence between $10^{-3}$ and $10^{-2}$ $L_\odot$ did so within only a few hundred million years. "Stars" in the transition region do ignite hydrogen even if they will eventually fizzle into brown dwarfs.

Figure 6 contrasts the evolution of the ratio of the nuclear luminosity to the total luminosity ($L_n/L$; see Tables 3–9) in models C (high-opacity) and E (low-opacity) for $M$ = 0.06, 0.07, 0.075, 0.085, 0.09, 0.095, and 0.1 $M_\odot$. As Figure 6 shows, even though the lower mass models in the series will eventually settle to $L_n/L = 0.0$ and be brown dwarfs, $L_n/L$ can be near 50% for billions of years. Indeed, an object "at" the precise edge of the main sequence will take an infinite amount of time to reach it (D'Antona and Mazzitelli 1985). For illustration, we note that for models A–D, the 0.08 $M_\odot$ stars that just make the main sequence do so ($L_n/L = 1.0$) only after $\sim$40 Gyr. This is significantly longer than the age of the universe. Since "stars" that will eventually miss the main sequence can for billions of years derive a large fraction of their luminosity from the thermonuclear burning of hydrogen and since those objects that will eventually land on the main sequence may take a time in excess of the age of the universe to do so, the *precise* main-sequence mass limit has little observational significance. In the main-sequence transition region, the age is as important a feature as the luminosity and effective temperature when comparing theory with observation and diagnosing the family of low-mass objects. Whether a "star" is thermonuclear is not a direct observable (save through deuterium and lithium depletion). This extra degree of freedom (age) complicates, yet enriches, the study of the VLM/BD continuum.

As Figure 5 demonstrates, the models fit most of the luminosity versus mass data reasonably well, though one model is not obviously selected over others by this plot. Figure 7 depicts luminosity versus mass isochrones at ages $10^8$, $10^9$, and $10^{10}$ yr for high-opacity models B ($\alpha = 1.0$) and D ($\alpha = 0.1$). Superposed are some results from other theorists (Grossman, Hayes, and Graboske 1974; Vandenberg *et al.* 1983; D'Antona and Mazzitelli 1985) and the data from LP87 and Mc88. As Figure 7 suggests, the high-luminosity, low-mass data points of LP87 that do not easily fit the Figure 5 isochrones at $10^{10}$ yr (GL 473AB, GL 748B, GL 234B) can easily fit younger isochrones ($\sim 10^8$ yr). If this explanation becomes problematic, systematic underestimates in the observed masses or overestimates in the observed luminosities should not be ruled out. If these observations are upheld and these objects are shown to be old ($> 10^9$ yr), then high opacities in the $< 2600$ K regime that can extend the main sequence, as explained below, are indicated. Be that as it may, most of the data fit the theory (e.g., model B) surprisingly well.

Note that as Figure 7 shows, the luminosities continue to

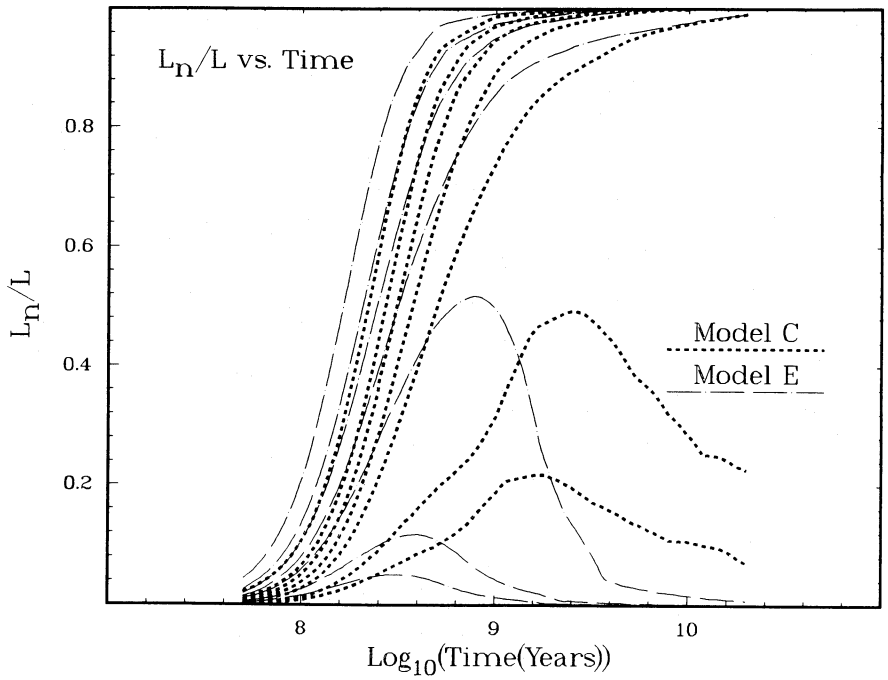


FIG. 6.—The ratio ($L_n/L$) of the nuclear luminosity to the total luminosity vs. age for high-opacity model C ($\alpha = 0.5$) and low-opacity model E ($\alpha = 0.5$) for seven masses (0.1, 0.095, 0.09, 0.085, 0.075, 0.07, and 0.06 $M_\odot$). The bifurcation between the VLM and BD branches is manifest, as is the difference between low and high opacity. High-mass stars (*middle left*) reach the main sequence ($L_n/L$) quickly ($< 10^9$ yr) while low-mass stars ($\leq 0.07\ M_\odot$) burn hydrogen for a time and then fizzle out ($L_n/L \rightarrow 0.0$).

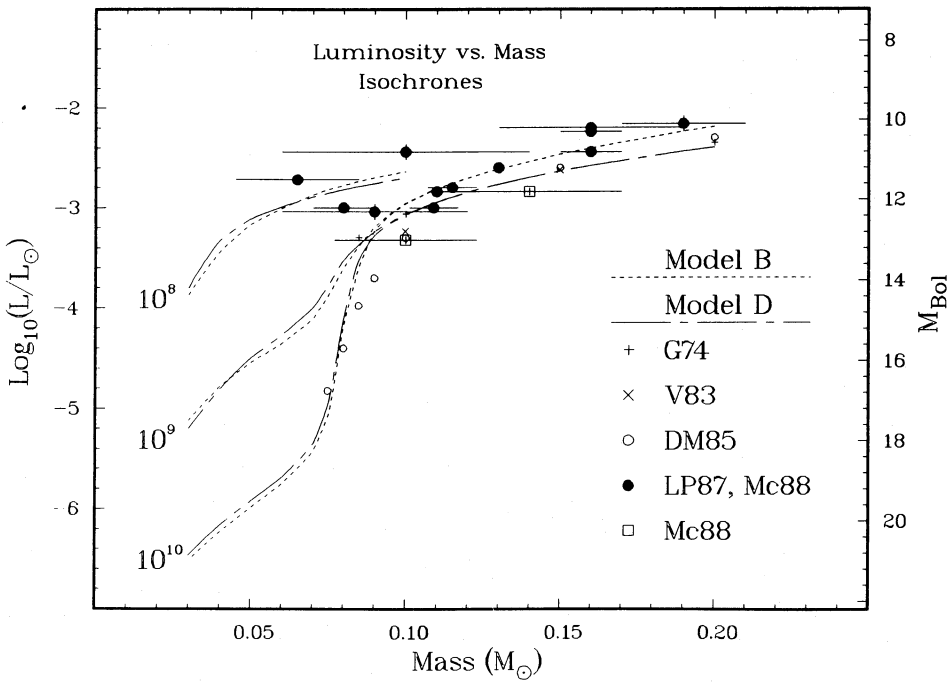


FIG. 7.—Luminosity (in units of $L_\odot$) and $M_{bol}$ ($M_{bol}(\odot) = 4.70$) vs. Mass (in $M_\odot$) isochrones at $10^8$, $10^9$, and $10^{10}$ yr for models B (*dash*; $\alpha = 1.0$) and D (*chain dash*; $\alpha = 0.1$). Also included are various theoretical points from G74 (*plus signs*), V83 (*crosses*), and DM85 (*open circles*; $5 \times 10^9$ yr) and the LP87 and Mc88 data. See text for discussion.

collapse with time ($L \propto 1/t^{1.0}$) in the brown dwarf regime, as they cannot ignite hydrogen to stabilize their surface losses. At higher masses, the isochrones converge, indicating that as mass increases, the main sequence is more and more quickly reached. The region of bifurcation between continued cooling at low masses and rapid stabilization at "high" masses is the main-sequence transition zone.

Shown in Table 10 are the approximate values of the minimum main-sequence mass (MMSM), luminosity (MMSL), and effective temperature (MMST) for the full gamut of models A–G. For all models save model E, MMSL is very close to 0.08 $M_\odot$, a number found elsewhere in the literature (D'Antona and Mazzitelli 1985; Kumar 1963*a*, *b*; Grossman Hays, and Graboske 1974). For the high-opacity, low-$Y_\alpha$ (=0.22) models A–D, MMSL is $\sim 6.0 \times 10^{-5}\ L_\odot$ ($M_{\rm bol} \sim 15$) and MMST is 1700–1800 K, regardless of the mixing-length parameter, which for these models ranges from $\infty$ to 0.1 (see Table 2). However, for the high-opacity, "high"-$Y_\alpha$ (0.25) model G, MMSL is approximately twice and MMST is $\gtrsim 300$ K larger than the corresponding quantities for models A–D. In addition, the $L$ versus $M$ curve begins its transition from BD to VLM at a very slightly lower mass for the higher $Y_\alpha$ models (see model G in Fig. 5).

As Table 10 indicates, MMSM for the low-opacity model E is $\sim 5.1 \times 10^{-4}\ L_\odot$ and MMST is $\sim 2870$ K, all larger than the corresponding quantities for the other models. Furthermore, as Figure 5 demonstrates, model E luminosities are above those of the other models on the main sequence, but fall below them in the brown dwarf regime. In addition, for model E the transition from BD to VLM is exceedingly abrupt (Fig. 5). The behavior of model E serves to demonstrate the effect of opacity in VLM/BD's. Lower opacity allows one to peer deeper into the star to higher temperatures. The higher effective temperatures lead to higher luminosities on the main sequence. However, the higher luminosities require higher central temperatures ($T_c$) to maintain them by thermonuclear burning. Such high $T_c$'s are less easily achieved with a less insulating, low-opacity blanket. Therefore, as the mass decreases along the VLM sequence, the low opacity models will slide off the main sequence sooner, at higher MMSMs, MMSLs, and MMSTs. Furthermore, low-opacity brown dwarfs will, by dint of their higher transparency, cool more quickly to lower luminosities and temperatures. Hence, the lower luminosity brown dwarfs and higher luminosity VLMs seen in model E can both be explained by the low opacity of model E alone. This low-opacity effect explains the positions of low-metallicity (Population II) subdwarfs on the H-R diagram (D'Antona 1987). Conversely, a higher opacity leads to lower luminosities and effective temperatures on a main sequence that can extend to lower masses before falling onto the brown dwarf branch.

TABLE 10

MINIMUM MAIN-SEQUENCE VALUES FOR MASS (MMSM), LUMINOSITY (MMSL), AND EFFECTIVE TEMPERATURE (MMST)

| Model | MMSM ($M_\odot$) | MMSL ($L_\odot$) | MMST (K) |
|---|---|---|---|
| A..... | ~0.08 | $6.0 \times 10^{-5}$ | 1730 |
| B..... | ~0.08 | $6.2 \times 10^{-5}$ | 1740 |
| C..... | ~0.08 | $6.2 \times 10^{-5}$ | 1740 |
| D..... | ~0.08 | $7.2 \times 10^{-5}$ | 1800 |
| E..... | ~0.09 | $5.1 \times 10^{-4}$ | 2870 |
| F..... | ~0.08 | $6.0 \times 10^{-5}$ | 1730 |
| G..... | ~0.08 | $1.3 \times 10^{-4}$ | 2100 |

Decreasing $\alpha$ should decrease the efficiency of convection and result in lower luminosities and lower effective temperatures, all else being equal. The actual effect of changing the mixing-length parameter ($\alpha$) on the luminosity versus mass curves is easily gleaned from Figures 5 and 7, Table 10, and Tables 3–6, in which models A ($\alpha = \infty$), B ($\alpha = 1.0$), C ($\alpha = 0.5$), and D ($\alpha = 0.1$) for the high opacity case are summarized. We see that the luminosity is indeed a monotonically increasing function of $\alpha$ in the VLM regime, changing by a factor of $\sim 1.5$ from model D to model A. While models B ($\alpha = 1.0$) and C ($\alpha = 0.5$) are not much different, the differences between models B and D ($\alpha = 0.1$), where $\alpha$ has changed by a factor of 10, are pronounced. For these models, the 0.2 $M_\odot$ $T_e$'s differ by $\sim 400$–500 K, while $L_{\rm B}$ is more than 50% higher than $L_{\rm D}$. Indeed, VLM behavior is more dependent on $\alpha$ (models A–D) than on opacity (model C vs. model E). In the brown dwarf regime, the effect of varying $\alpha$ is minimal (the convective velocities are already low and hydrogen dissociation and ionization do not play a role in the transition from radiative to convective energy transport), and models A–D are roughly degenerate.

### *b) Effective Temperature*

While the $\alpha$ dependence is less obvious on log $L$ versus mass plots such as Figure 5, it is pronounced on $T_e$ versus mass plots. In Figure 8, $T_e$ versus mass at $10^{10}$ yr for models A–E and model G is graphed. Superposed are the data of LP87. These data make clearer why we thought it important to explore the effect of varying $\alpha$. The effective temperatures range $\sim 600$ K at 0.2 $M_\odot$ from a low of 3010 K for model D ($\alpha = 0.1$) to a high of 3620 K for model A ($\alpha = \infty$). The actual data in the VLM region are bracketed by models B ($\alpha = 1.0$, $Y_\alpha = 0.22$) or G ($\alpha = 1.0$, $Y_\alpha = 0.25$) and low-mixing-length model D ($\alpha = 0.1$). The low opacity model E along with high-opacity model A ($\alpha = \infty$) seem to be too hot to fit the LP87 data. As Berriman and Reid (1987) have shown, the existence of $H_2O$ absorption features and the intrinsic limitations of converting color bands and color temperatures to effective temperatures can lead to systematic and large (hundreds of K) errors in the data not reflected in the statistical error bars of Figure 8. Such large ambiguities should encourage more and better infrared *spectra* to be taken of VLMs and brown dwarf candidates so that systematic errors in both $T_e$ and $L$ do not long confuse comparisons with theory.

The $T_e$ versus $M$ curves of Figure 8 recapitulate the trends in the $L$ versus $M$ curves of Figure 5 already described above. In Figure 9 we compare the $T_e$ versus $M$ isochrones for models B and D at $10^8$, $10^9$, and $10^{10}$ yr with the LP87 $T_e$ data. As before (Fig. 7), the low-mass end of the data set may be explained by either youth, mass underestimation, or higher opacity below 2600 K. Furthermore, there should be a significant selection bias for high-luminosity, young objects in this low-mass range ($<0.08\ M_\odot$) where objects cool very quickly into obscurity. Nevertheless, the theory fits the data passably well. Note, however, that high-opacity, high-$\alpha$ models overlap with low-opacity, low-$\alpha$ models in the VLM range, though MMSM is sensitive to opacity alone. Therefore, the sheaf of models A–G serve only to point to the future final reconciliation of theory with data and not yet to the final model. To further illustrate this, we superpose on Figure 9 $T_e$ versus M points, where available, of other theorists (G74, V83, DM85). Encouragingly, we can be firm on one thing: objects with effective temperatures below $\sim 1500$ K and luminosities below $6 \times 10^{-5}$ $L_\odot$ are very probably brown dwarfs.

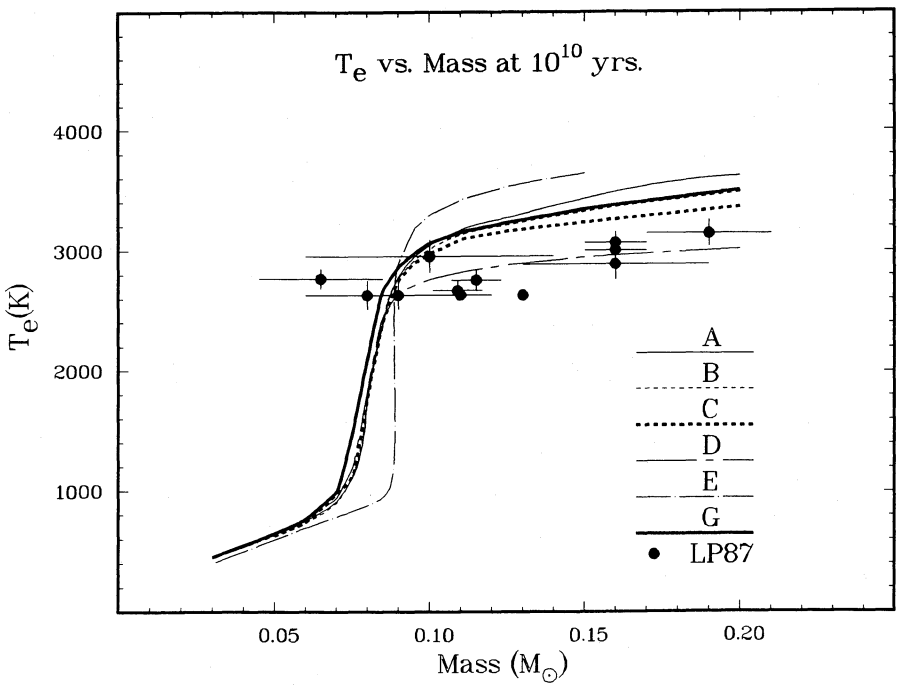


FIG. 8.—Effective temperature ($T_e$) vs. mass (in $M_\odot$) for models A through E and model G at $10^{10}$ yr. The LP87 data are superposed for comparison. The brown dwarf branch is in the lower left, and the VLM branch is in the upper right.

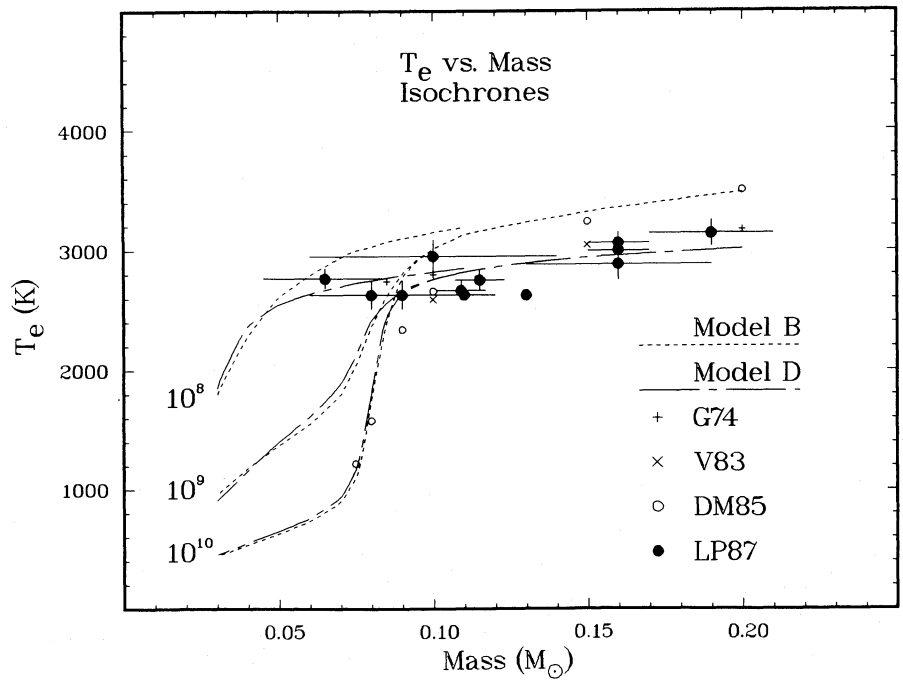


FIG. 9.—Effective temperature ($T_e$) vs. mass (in $M_\odot$) isochrones at $10^8$, $10^9$, and $10^{10}$ yr for models B (*dash*; $\alpha = 1.0$) and D (*chain dash*; $\alpha = 0.1$). Also shown are various theoretical points from G74 (*plus signs*), V83 (*crosses*), DM85 (*open circles*; $5 \times 10^9$ yr), and the LP87 data. The two models are seen to bracket the data. See text for discussion.

To show that our high opacity and the Alexander, Johnson, and Rypma (1983) opacities yield similar results, we compare the $T_e$ versus mass isochrones of models A (high opacity, $\alpha = \infty$) and F (Alex83 opacity, $\alpha = \infty$) in Figure 10. As this figure and Tables 4 and 8 demonstrate, the differences are not striking. In addition, to show that the VLM/BD continuum is not sensitive to the helium fraction, we reproduce in Figure 11 similar isochrones for models B ($Y_\alpha = 0.22$) and G ($Y_\alpha = 0.25$). Though, as Table 10 reveals, MMST is an interesting function of $Y_\alpha$, no "simple" observable can be easily used to indirectly obtain $Y_\alpha$, and good spectra are probably required for the task.

### c) *Structural Quantities*

A very important quantity derived by the theory and inferred from observations is the radius ($R$) of the star, plotted as a function of mass for models A–E and model G at $10^{10}$ yr in Figure 12. Also included are the radii derived by other theorists (G74; V83; DM85; and Rappaport and Joss 1984, hereafter RJ84), those radii obtained from the LP87 data set (without error bars), and $10^8$ year isochrones for extreme models D and E. We see immediately the natural separation between the low-mass, brown dwarf behavior and the high-mass, VLM behavior and the position and width of the transition region between the branches. There is a minimum radius in the VLM/BD continuum that, for cosmological helium fractions, is $\sim 0.07\ R_\odot$. The inverse $R$ versus $M$ behavior of brown dwarfs at $10^{10}$ yr reflects the corresponding white dwarf relation, since electron degeneracy pressure overwhelms thermal pressure at the high densities and low entropies on the old BD branch. Similarly, VLMs are supported mainly by thermal pressure and their radii show the exponential rise with entropy characteristic of ideal gas, $n = 1.5$ polytropes. For VLMs, radii are proportional to $M^{0.8}$ and are near 0.2–0.25 $R_\odot$ at $M = 0.2\ M_\odot$, and near 0.1 $R_\odot$ at $M = 0.09\ M_\odot$. Young stars ($\lesssim 10^8$ yr), quite naturally, have larger radii, as radiation during Kelvin-Helmholtz phases implies shrinkage, but final radii are early established for the more massive VLMs. Only for the objects below 0.1 $M_\odot$ can the radii evolve appreciably over time scales in excess of a few hundred million years.

As Figure 12 demonstrates, the LP87 radii do not fit any of the theories well (especially for GL 866A, GL 748B, GL 473AB, and GL 896B). They reside 20%–50% above the $10^{10}$ yr isochrones, through a few of the lower mass detections do fit $\sim 10^8$ yr isochrones, as expected. A discrepancy between theoretical and experimental radii has persisted for the last 15 yr (see Grossman, Hays, and Graboske 1974) and is the major obvious blemish on an otherwise useful theory. Though youth and selection effects might explain some of the problem, it would seem that the EOS is not to blame. Despite the wide range of EOSs employed by the other workers whose results are given in Figure 12, their $R(M)$ relationships are similar. While it is true that decreasing $\alpha$ or increasing the opacity increases VLM radii, the effect is not strong. Therefore, we conclude that the theoretical radii, since they are simply derived, are indeed under control and that mass underestimates, $T_e$ overestimates, and, in some cases, youth are the culprits. The radii have not, in general, been directly measured, but are indirectly derived from the difficult-to-obtain $T_e$ and $L$ estimates. Indeed, when one considers the squared-dependence on $T_e$ of the inferred radius at a given $L$ and the difficulty in deriving $T_e$, as well as age, it is encouraging that the data are anywhere near the theories depicted in Figure 12. When the radius of a low-mass secondary has been directly derived, as for the dwarf nova system Z Cha (Wade and Horne 1988), youth and/or binary interaction readily reconcile theory with observation. However, such direct observations are rare, and

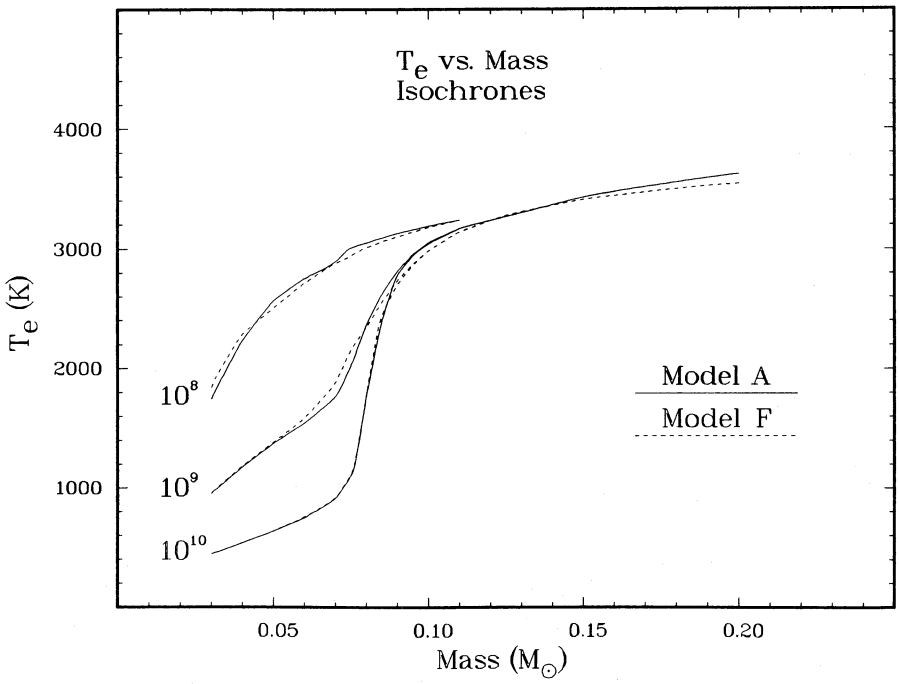


FIG. 10.—Effective temperature ($T_e$) vs. mass isochrones for models A (*solid*) and F (*dash*) at $10^8$, $10^9$, and $10^{10}$ yr. Model A has $\alpha = \infty$, $Y_\alpha = 0.22$, and our preferred opacities, while model F has $\alpha = \infty$, $Y_\alpha = 0.22$, and the Alexander, Johnson, and Rypma (1983) opacities. There is little difference between the two. See text for discussion.

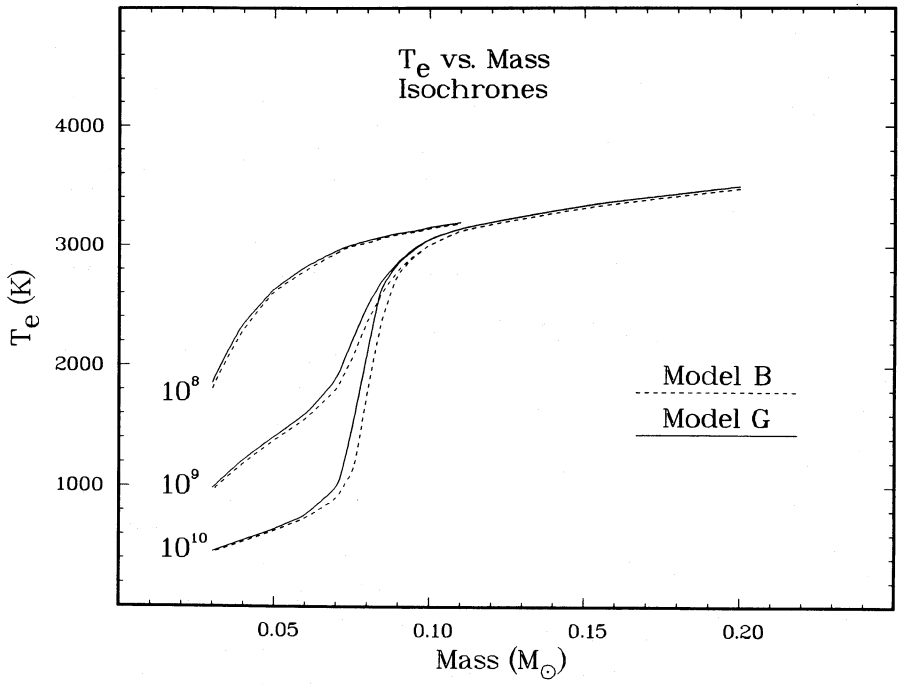


FIG. 11.—Effective temperature ($T_e$) vs. mass (in $M_\odot$) isochrones at $10^8$, $10^9$, and $10^{10}$ yr for models B (*dash*; $Y_\alpha = 0.22$) and G (*solid*; $Y_\alpha = 0.25$). The curves are superposed to discern the effect of changing the helium fraction, $Y_\alpha$. Aside from a slight leftward shift of model G relative to model B, there is little to distinguish one from the other.

observers are encouraged to do everything possible to accurately pin down the radii of VLMs and candidate brown dwarfs.

The evolution of the central temperature ($T_c$) above and below the edge of the hydrogen main sequence ($0.07\ M_\odot < M < 0.11\ M_\odot$) is shown in Figure 13 for models C (high opacity, $\alpha = 0.5$) and E (low opacity, $\alpha = 0.5$). Though $T_c$ is not an observable, its values and evolution reflect well the underlying physics of VLM's and brown dwarfs.

The differences in behavior between the brown dwarf and the VLM branches are apparent in Figure 13 and echo the trends of Figure 6. At early times ($< 10^8$ yr), all the "stars" are

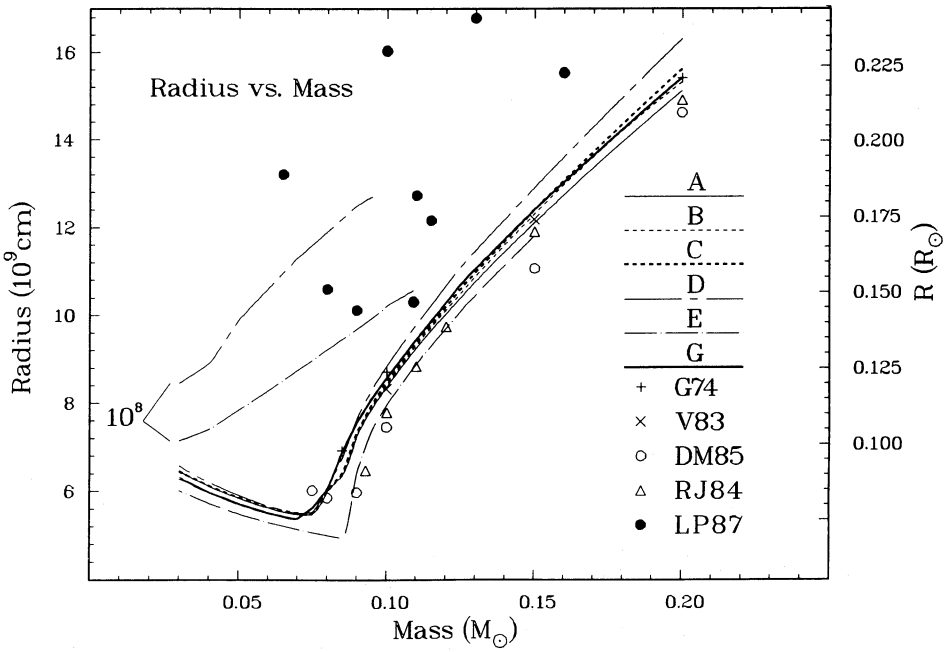


FIG. 12.—Radius (in units of $10^9$ cm [*left*] and $R_\odot$ [*right*]) vs. mass (in $M_\odot$) for models A through E and model G. Also shown are $10^8$ yr isochrones for models D (*chain dash*) and E (*chain dot*), some theoretical points from other workers (G74 [*plus signs*], V83 [*crosses*], DM85 [*open circles*], and RJ84 [*open triangles*]) and the LP87 data, without error bars. Three of the LP87 points are off the graph. The brown dwarf branch is clearly discernible in the lower left, while the VLM main sequence dominates the center and right. Note that the ordinate is linear, not logarithmic and that it starts, not at $R = 0.0$, but at $R = 4 \times 10^9$ cm. See text for further discussion.

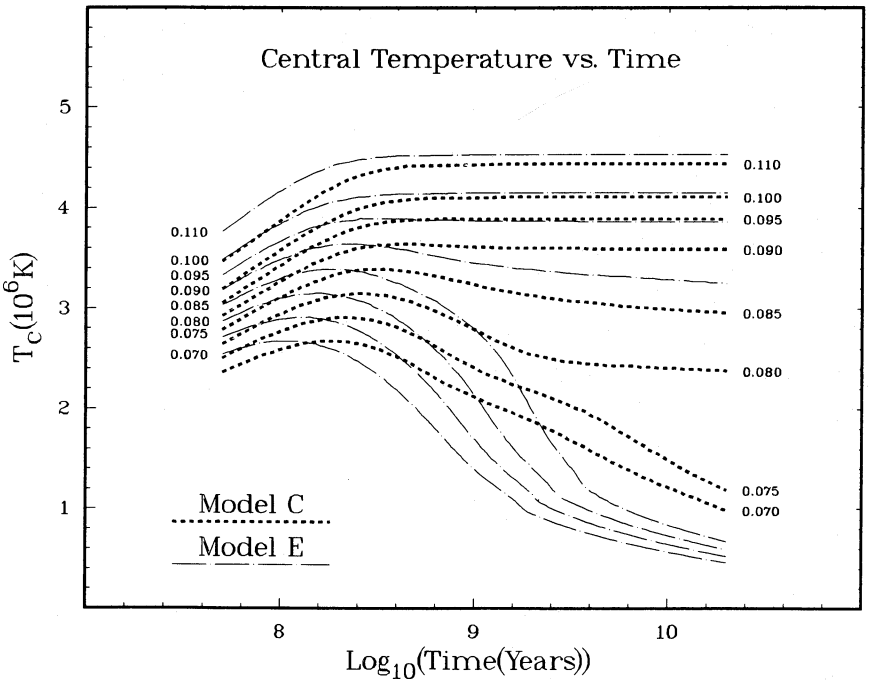


FIG. 13.—Central temperature ($T_c$, in units of $10^6$ K) vs. age (time, in years) for eight "stars" with masses 0.07, 0.075, 0.08, 0.085, 0.09, 0.095, 0.1, and 0.11 $M_\odot$ for models C (*dot*; high-opacity) and E (*chain dot*; low-opacity). The curves are indexed by mass on the left (model E) and on the right (model C) of the appropriate curve. See text for discussion.

in their Kelvin-Helmholtz settling phase and $T_c$ rises by the normal negative specific heat effect. If the object's mass is too low, it will become degenerate before it can ignite hydrogen and balance its surface losses. The $T_c$'s of such "stars" below the edge of the main-sequence peak turn around and decline on a degenerate brown dwarf cooling curve. The $T_c$ of a star whose mass is just above the edge of the main sequence peaks *above* the final $T_c$ at which it will eventually stabilize on the main sequence, but it does stabilize. However, the $T_c$'s of more massive stars ($\gtrsim 0.1\ M_\odot$) peak and stabilize simultaneously and earlier.

As Figure 13 shows, the bifurcation in $T_c$ evolutionary behavior between VLM and brown dwarf branches occurs at higher masses for the lower opacity model E, for which the main sequence $T_c$'s are also slightly higher, as explained above.

Stars just above the main-sequence edge can stabilize at temperatures below the peak temperature they achieve because, as they evolve those last billions of years, they continued to settle and contract. The increasing $\rho_c$ compensates in the rate of process (1) for the slight decrease in $T_c$. In this way, $L_n/L$ is indeed a monotonically increasing function of time (after deuterium burning) above the main-sequence edge.

The central density ($\rho_c$) versus mass at $10^{10}$ yr is depicted in Figure 14 for models A–E and model G. Included are corresponding numbers derived by other theorists (G74, V83, DM85, RJ84). The VLM/BD transition region is well marked by the peak in $\rho_c$. For high-opacity models (A–D, G), $\rho_c$ peaks near 1000 g cm$^{-3}$. However, the peak $\rho_c$ for low opacity model E is appreciably higher ($\sim$1700 g cm$^{-3}$). Such behavior is quite naturally allied with the smaller radii seen in Figure 12 for model E. Note that not only are the $\rho_c$'s of other theorists comparable to ours, but that $\rho_c$ is not a sensitive function of $\alpha$ (compare models A–D). This serves to punctuate our conclusion above that the problems with the radii are not to be solved by modifications in the EOS.

### *d) H-R Diagrams*

One of the best ways to display numerical results is with luminosity versus effective temperature plots (H-R diagrams). The classic format allows a direct comparison with the primary observables. Figure 15 is an H-R diagram of low-opacity model E ($\alpha = 0.5$) and high-opacity, low-$\alpha$ model D ($\alpha = 0.1$) at an age of $10^9$ yr. Note that the temperature scale is linear. These particular models were chosen because they, of the seven models of Table 2, differ the most and, between the two of them, claim the most territory on the H-R diagram. The positions of the 14 "stars" between 0.03 $M_\odot$ and 0.15 $M_\odot$ are indicated by small solid dots on the model lines, and their masses are written to the left of the model E (*lower*) line. Solid "isomass" lines are drawn between the model lines for ready comparison. Also drawn are lines of constant radius (0.15, 0.2, and 0.3 $R_\odot$). To these results of theory are added the LP87, BR87, and BZ88 data from Figure 1, which should be referred to when the names of the observed M (or brown) dwarfs are needed.

Figure 15 shows that there is a disturbing lack of overlap between the BZ88 data and either the LP87 or the BR87 data. The BZ88 points (GD 165B, LHS 2924, GL 569B, VB 8, and VB 10) are at systematically lower radii and do approximately conform to the model E line. However, BZ88 have made no corrections in their $T_e$ estimates for the water absorption feature, that BR87 have shown are important. Indeed, BZ88 obtain effective temperatures for VB 8 and LHS 2924 that are higher than the values derived by BR87 for the same stars by $\sim$650 K and $\sim$900 K, respectively, and they derive an effective temperature for GL 569B that is $\sim$300 K higher than that

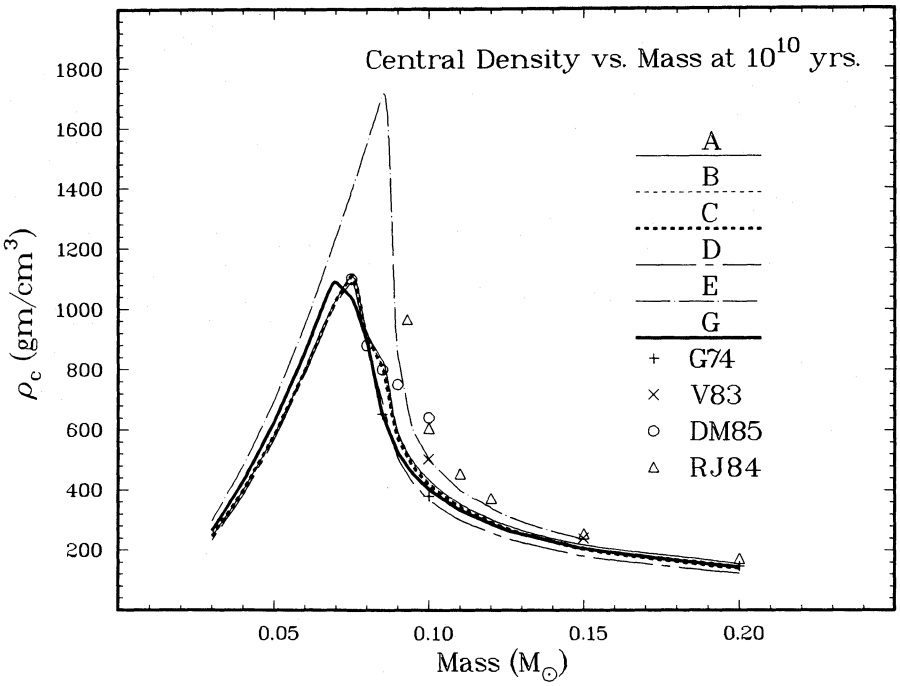


FIG. 14.—Central density ($\rho_c$, in cgs) vs. mass (in $M_\odot$) at $10^{10}$ yr for models A through E and model G. Also included are a few theoretical points gleaned from the literature (G74 [*plus signs*], V83 [*crosses*], DM85 [*open circles*], RJ84 [*open triangles*]). Note that, while $\rho_c$ is not a strong function of the helium fraction or the mixing length parameter, that it is a strong function of the opacity around the transition region between VLMs (*right*) and BDs (*left*).

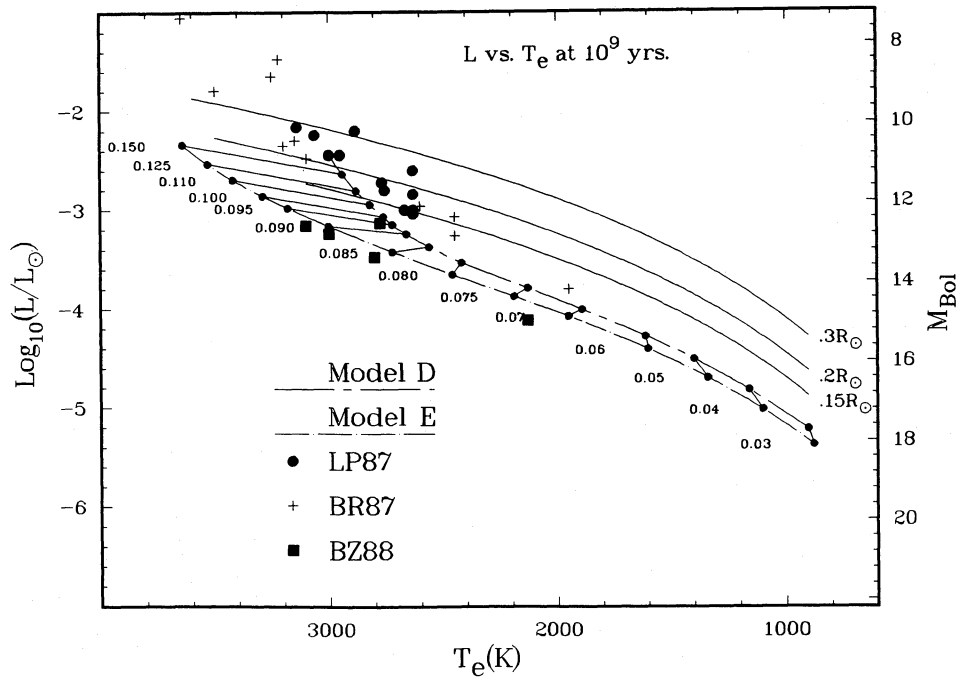


FIG. 15.—H-R diagrams (luminosity [$L$] vs. effective temperature [$T_e$]) for high-opacity model D ($\alpha = 0.1$) and low-opacity model E ($\alpha = 0.5$) at $10^9$ yr. The $T_e$ scale is linear. Superposed are the LP87, BR87, and BZ88 data from Fig. 1. The right ordinate is bolometric magnitude [$M_{bol}(\odot) = 4.70$]. Solid lines of constant radius at 0.15, 0.2, and 0.3 $R_\odot$ are included. Each of the 14 "stars" per model is marked with a small solid dot, and equal mass lines connect the corresponding points for models D and E. The value of the mass is given to the left of the model E isochrone. See text for discussion.

obtained by Forrest, Skrutskie, and Shure (1987) (see Table 1). While we are loath to judge which data set is the more accurate, discrepancies between the "corrected" BR87 data and the uncorrected BZ88 data alone suggests that there are systematic errors in the extant $T_e$ data. Interestingly, as the $5 \times 10^9$ yr isochrone on Figure 16 for standard ($\alpha = 1.0$) high-opacity model B amply demonstrates, this model bisects the BZ88 and LP87/BR87 data while avoiding both. Lowering the BZ88 $T_e$'s by $\sim$200–300 K and raising the LP87/BR87 $T_e$'s by $\sim$200–400 K would bring all the data into line with a canonical model without "tampering" with $\alpha$.

However, as both Figures 15 and 16 demonstrate, a decrease in $\alpha$ to $\sim$0.1 (model D) does indeed lift the theoretical line in radius up into where much of the LP87 and BR87 data now reside. The curvature of the theoretical H-R line in the VLM regime is a direct mapping of the temperature (or opacity) versus pressure profile in the atmosphere of the star (see Figs. 3 and 4). For the lower mixing-length parameters, the radiative gradient stays superadiabatic deep into the skin to pressures and temperatures ($>10^4$ K) for which our opacity algorithm (and those of others) is suspect. Improved opacity algorithms in this problematic deep regime may straighten the model D H-R line to conform more to all the LP87 and BR87 data, but the low-$\alpha$ effect we see in Figures 15 and 16 is suggestive. As discussed in § II*c*, $\alpha$ may well be of order 0.1 in brown dwarfs as well, but they are not sensitive to this parameter. The physical basis for low mixing lengths is uncertain; one possibility is that low mixing lengths simulate in a crude way the suppression of convection by strong magnetic fields. However, to test such a speculation would require much more detailed modeling. If the BZ88 data should prove closer to the mark, even after the required corrections, low $\alpha$'s may not be necessary. In this case, our standard models B or G would be indicated.

As Figures 15 and 16 show, whatever the value of $\alpha$ on the VLM branch, its precise value below the main-sequence edge, on the brown dwarf branch, is not important. "Stars" below $\sim$0.075 $M_\odot$ slide down what are roughly constant radius trajectories (see also Fig. 12) to lower luminosities and effective temperatures. Curiously, we find that GD 165B, LHS 2924, and GL 569B could easily be VLMs and need not be brown dwarf candidates (see Table 10 and D'Antona and Mazzitelli 1985). Furthermore, Figures 15 and 16 suggest that the BR87 objects GL 884, GL 752A, GL 411, and GL 821 and the LP87 objects GL 53B, GL 896B, and GL 166C are each in fact more massive than the 0.2 $M_\odot$ upper limit to our study.

## IV. CONCLUSIONS

The VLM/BD continuum poses formidable theoretical and observational challenges. In this paper, we have presented and described seven models, each represented by 15 objects with masses between 0.03 and 0.2 $M_\odot$, that explore in a self-consistent and detailed way the physics of $M$ dwarfs just above and brown dwarfs just below the hydrogen main-sequence cutoff. We investigated the dependence of the luminosities, effective temperatures, radii, etc. on mixing length, helium fraction, and atmospheric opacity and compared the recent data with our calculations. Our theory in the VLM range generally fits the data, but the inferred radii in particular are problematic. This problem can be solved for the LP87/BR87 data sets, if low values ($\sim$0.1) of the mixing-length parameter ($\alpha$) are evoked for the lower mass VLMs but systematic errors in the observed effective temperatures, masses, and luminosities may well be the culprits. In particular, corrections of only a few hundred K in $T_e$ would bring the BZ88 data comfortably into line with our standard models B and G. Furthermore, the possibility that rapid rotation is involved should not be discounted (D'Antona 1987). The centrifugal effect on the effective radius of a rapidly rotating VLM may be large and may be

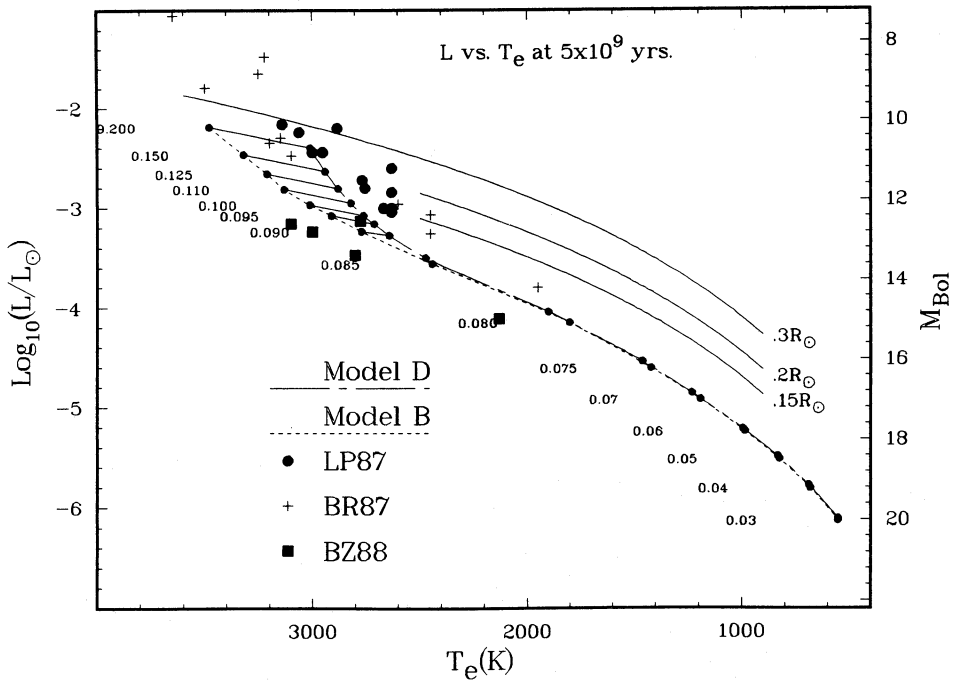


FIG. 16.—Same as Fig. 15 but for models B and D and including $M = 0.2\ M_\odot$. These models have the same opacity algorithm and helium fraction but different mixing-length parameters ($\alpha = 1.0$ and 0.1 respectively). See text for discussion.

connected with the coronal activity of some M dwarfs. Nevertheless, our models illuminate the character of the VLM/BD transition region and point to further ways to reconcile the remaining minor discrepancies between theory and observation.

The recent brown dwarf candidates (e.g., GL 569B, Giclas 29–38, GD 165B, and LHS 2924) are tantalizing, but unproven. Crucial to further progress in this field are more and better IR spectra of objects below 2500 K. Good spectra and new theoretical spectral syntheses for these high-gravity "stars" (work in progress), along with deeper, more complete photometric surveys should soon allow us to determine whether baryonic matter in the form of VLMs and/or brown dwarfs exists in Galactic or cosmologically interesting quantities. The dark matter problems aside, revealing the nature of dim stars and brown dwarfs remains a fascinating problem at the forefront of stellar evolution theory.

The authors would like to thank T. Henry, J. Liebert, G. Berriman, and D. McCarthy for useful conversations and tutorials on the new data and D. J. Stevenson for advice on the proper specific heats to use in the atmosphere models. Support through NSF grants AST87-14176 and AST86-08475 and by the Alfred P. Sloan Foundation (A. B.) is gratefully acknowledged.

## REFERENCES


Alexander, D. R. 1989, in preparation.
Alexander, D. R., Johnson, H. R. and Rypma, R. L. 1983, *Ap. J.*, **272**, 773.
Bahcall, J. N. 1986, *Ann. Rev. Astr. Ap.*, **24**, 577.
Becklin, E. E., and Zuckerman, B. 1988, *Nature*, **336**, 656 (BZ88).
Berriman, G., and Reid, N. 1987, *M.N.R.A.S.*, **227**, 315 (BR87).
Burrows, A., and Lattimer, J. M. 1986, *Ap. J.*, **307**, 178.
Cox, A. N., Shaviv, G., and Hodson, S. W. 1981, *Ap. J.* (*Letters*), **245**, L37.
D'Antona, F. 1987, *Ap. J.*, **320**, 653.
D'Antona, F., and Mazzitelli, I. 1985, *Ap. J.*, **296**, 502 (DM85).
Del Genio, A. D., and McGratten, K. B. 1988, *Bull. AAS*, **20**, 868.
Fontaine, G., Graboske, H. C., Jr., and Van Horn, H. M. 1977, *Ap. J. Suppl.*, **35**, 293 (FGVH).
Forrest, W. J., Skrutskie, M. F., and Shure, M. 1988, *Ap. J.* (*Letters*), **330**, L119.
Fowler, W. A., Caughlan, G. R., and Zimmerman, B. A. 1975, *Ann. Rev. Astr. Ap.*, **13**, 69 (FCZ).
Fruchter, A. S., Gunn, J. E., Lauer, T. R., and Dressler, A. 1988, *Nature*, **334**, 686.
Giclas, H. L. 1958, *Lowell Obs. Bull.*, **4**, 1.
Gliese, W. 1969, *Catalogue of Nearby Stars, Veröff. Astr. Recken.-Inst. Heidelberg*, No. 22.
———. 1974, *Astr. Ap.*, **34**, 147.
Graboske, H. C., DeWitt, H. E., Grossman, A. S., and Cooper, M. S. 1973, *Ap. J.*, **181**, 457.
Grossman, A. S. 1970, *Ap. J.*, **161**, 619.
Grossman, A. S., Hays, D., and Graboske, H. C. 1974, *Astr. Ap.*, **30**, 95 (G74).
Hawkins, M. R. S. 1986, *M.N.R.A.S.*, **223**, 845.
Hubbard, W. B., and DeWitt, H. E. 1985, *Ap. J.*, **290**, 388.
Kumar, S. 1963*a*, *Ap. J.*, **137**, 1121.
———. 1963*b*, *Ap. J.*, **137**, 1126.
Liebert, J., and Probst, R. G. 1987, *Ann. Rev. Astr. Ap.*, **25**, 473 (LP87).
Lunine, J. I., Hubbard, W. B., and Marley, M. S. 1986, *Ap. J.*, **310**, 238.
Lunine, J. I., Hubbard, W. B., Burrows, A., Wang, Y. P., and Garlow, K. 1989, *Ap. J.*, **338**, 314 (Paper I).
Lunine, J. I., and Hunten, D. M. 1987, *Icarus*, **69**, 566.
Luyten, W. J. 1963, *Proper Motion Survey with the 48 Inch Schmidt Telescope*, No. 1 (Minneapolis: University of Minnesota).
———. 1976*a*, *Proper Motion Survey with the 48 Inch Schmidt Telescope*, No. 46 (Minneapolis University of Minnesota).
———. 1976*b*, *LHS Catalogue* (2d ed.; Minneapolis: University of Minnesota).
Magni, G., and Mazzitelli, I. 1979, *Astr. Ap.*, **72**, 134 (MM).
Marley, M. S., and Hubbard, W. B. 1988, *Icarus*, **73**, 536 (MH).
Marcy, G. W., and Moore, D. 1989, *Ap. J.*, **341**, 961.
McCarthy, D. W., Jr., Cobb, M. L., and Probst, R. G. 1987, *A.J.*, **93**, 1535.
McCarthy, D. W., Jr., Henry, T., Fleming, T. A., Saffer, R. A., Liebert, J., and Christou, J. C. 1988*a*, *Ap. J.*, **333**, 943.
———. 1988*b*, preprint (Mc88).
Mihalas, D. 1978, *Stellar Atmospheres* (San Francisco: Freeman), p. 185.
Nellis, W. J., Mitchell, A. C., van Thiel, M., Devine, G. J., Trainor, R. J., and Brown, N. 1983, *J. Chem. Phys.*, **79**, 1480.
Oort, J. 1960, *Bull. Astr. Inst. Netherlands*, **15**, 45.
Probst, R., and Liebert, J. 1983, *Ap. J.*, **274**, 245.
Rappaport, S., and Joss, P. C. 1984, *Ap. J.*, **283**, 232 (RJ84).
Reid, N. and Gilmore, G. 1984, *M.N.R.A.S.*, **206**, 19.
Robnik, M., and Kundt, W. 1983, *Astr. Ap.*, **120**, 227 (RK).
Sarazin, C. L., and O'Connell, R. W. 1983, *Ap. J.*, **268**, 552.
Scalo, J. 1986, *Fund. Cosmic Phys.*, **11**, 1.
Stringfellow, G. 1986, in *Astrophysics of Brown Dwarfs*, ed. M. C. Katatos, R. S. Harrington, and S. P. Maran (Cambridge: Cambridge University Press), p. 190.
Tsuji, T. 1971, *Pub. Astr. Soc. Japan*, **23**, 553.
Vandenberg, D. A., and Bridges, T. J. 1984, *Ap. J.*, **278**, 679.
Vandenberg, D. A. Hartwick, F. D. A., Dawson, P., and Alexander, D. R. 1983, *Ap. J.*, **266**, 747 (V83).
Wade, R. A., and Horne, K. 1988, *Ap. J.*, **324**, 411.
Zuckerman, B., and Becklin, E. E. 1988, *Nature*, **330**, 138.


ADAM BURROWS: Departments of Physics and Astronomy, University of Arizona, Tuscon, AZ 85721

W. B. HUBBARD and J. I. LUNINE: Lunar and Planetary Laboratory, University of Arizona, Tucson, AZ 85721